

People's Democratic Republic of Algeria
Ministry of Higher Education and Scientific Research
University M'Hamed Bougara of Boumerdes



Institute of Electrical Engineering and Electronics

Dissertation

PRESENTED BY:

Abderraouf Benzerga

Mohammed Ridha Hamidani

In Partial Fulfilment Of The Requirements For The Degree Of
MASTER

Field: ELECTRONICS

Option: COMPUTER ENGINEERING - POWER ENGINEERING

**Design and Construction of a Bidirectional DC-DC
Converter**

JURY MEMBERS:

Supervisor name: Dr.Brahim Metidji

Academic Year: 2024/2025

N⁰ d'ordre..... /IGEE/UMBB

DEDICATION

In the name of Allah, the Most Gracious, the Most Merciful.

We dedicate this work:

*To our beloved parents,
for their unconditional love, patience, and countless sacrifices.*

*To our families,
for their encouragement, understanding, and prayers throughout this journey.*

*To our teachers and mentors,
whose guidance and knowledge have shaped our academic path.*

*To SARL Microtech,
for providing us with the tools, space, and support during our internship,
which allowed us to bring our project to life in practice.*

*And to all students who strive for excellence,
despite limitations and obstacles.*

Alhamdulillah for the strength, patience, and perseverance to complete this work.

ACKNOWLEDGMENT

We would like to sincerely thank our supervisor, **Dr. B. Metedji**, for his continuous support, expert guidance, and valuable feedback throughout the development of this project. His insightful comments and encouragement greatly contributed to both our technical growth and the overall direction of our work.

We are also grateful to the faculty and staff of the *Institute of Electric and Electronic Engineering* for providing a stimulating academic environment and access to essential resources.

Special thanks go to the team at **SARL Microtech**, where the hardware implementation of our converter was carried out as part of our academic internship. Their technical assistance and facilities played a crucial role in validating our experimental work.

Finally, we extend our heartfelt appreciation to our families and close friends for their patience, understanding, and moral support during this journey.

Abstract

Bidirectional DC-DC converters are essential in modern power electronics, enabling efficient bidirectional power flow required for electric vehicles, renewable energy integration, and advanced energy storage systems. This project presents the design, simulation, and practical implementation of a Dual Active Bridge (DAB) bidirectional DC-DC converter. The converter is simulated for operation between 48V input and 400V output, while the practical implementation is carried out with a 24V input and an output ranging from 48V upwards. The system utilizes phase-shift modulation for power regulation, and microcontroller is employed for digital control implementation. Simulation was conducted using PLECS to evaluate the system's performance and to optimize key design parameters prior to hardware implementation. A phase-shift control strategy incorporating a PI controller was implemented in the simulation to investigate the bidirectional power flow capability of the converter. In the experimental phase, the DAB converter was tested under varying phase-shift values to assess its power transfer behavior and validate bidirectional operation. The experimental results closely aligned with the simulation outcomes, confirming the effectiveness of the control strategy and the successful realization of bidirectional power flow. The results contribute to the development of high-performance bidirectional converters for future power electronics applications.

Keywords: Bidirectional DC-DC Converter, Dual Active Bridge, Phase-Shift Modulation, TI C2000, PLECS Simulation, Energy Storage, Power Electronics.

CONTENTS

List of Variables	xii
1 Literature Review	
Bidirectional DC-DC Converter	2
1.1 Introduction to Bidirectional DC-DC Converters	2
1.2 Non-Isolated Bidirectional DC-DC Converter Topologies	3
1.2.1 Buck and Boost Derived Topology	3
1.2.2 Buck-Boost Derived Topology	3
1.2.3 ĆUK Derived Topology	4
1.2.4 SEPIC and Zeta Derived Topology	4
1.2.5 Cascade Topology	5
1.2.6 Switched-Capacitor Topology	5
1.2.7 Interleaved Topology	6
1.2.8 Multilevel Topology	6
1.3 Isolated Bidirectional DC-DC Converter Topologies	7
1.3.1 Flyback Topology	7
1.3.2 Isolated ĆUK Topology	7
1.3.3 Push-Pull Topology	8
1.3.4 Forward Topology	8
1.3.5 Dual Active Bridge (DAB) Topology	8
1.3.6 Dual Half-Bridge Topology	9
1.3.7 Half-Bridge to Full-Bridge Topology	9
1.3.8 Multiport DAB Topology	10
1.4 Comparison Between Isolated and Non-Isolated Bidirectional DC-DC Converters	10
1.5 Comparison Between Isolated Bidirectional DC-DC Converter Topologies	11
1.6 Why the Dual Active Bridge is a Preferred Topology	12
1.7 Control Strategies for Bidirectional DC-DC Converters	13

CONTENTS

1.7.1	Single Phase Shift (SPS) Control	13
1.7.2	Alternative Control Strategies	13
2	DAB Converter System Design	15
2.1	System Overview	15
2.2	Dual Active Bridge Analogy With Power Systems	16
2.3	Fundamental Working of the DAB Converter	17
2.4	Transformer Design and Leakage Inductance Considerations	20
2.5	Output Capacitor Selection	21
2.6	Control System	22
2.6.1	Dynamic Modeling and Control	22
2.6.2	Control Architecture	23
2.7	Losses in DAB Converter	24
3	Simulation	25
3.1	Objectives of the Simulation	25
3.2	Simulation Tools Used	25
3.3	System Parameters	25
3.4	Simulation Model Overview	26
3.5	Controller Design and Implementation	26
3.6	Phase Shift Calculation	27
3.7	Control System Description	27
3.7.1	Voltage Loop Equation	28
3.7.2	Current Loop Equation	28
3.7.3	PI Controller Gains	28
3.8	Simulation Scenarios and Results	28
3.8.1	Steady-State Operation	28
3.8.2	Conclusion and Waveform Analysis for forward Mode(48 V to 400 V)	31
3.8.3	Conclusion and Waveform Analysis for reverse Mode (400 V to 48 V):	35
3.9	Discussion	35
4	Experimental Implementation	37
4.1	Construction of the DAB Converter	37
4.2	Transformer Testing	38
4.2.1	Transformer Description	38
4.2.2	Transformer Windings	39
4.2.3	Leakage Inductance Measurement	39
4.2.4	Addition of External Leakage Inductance	39
4.2.5	Primary and Secondary Voltage Testing	40
4.3	Materials and Equipment Used	41

CONTENTS

4.4	Experimental Setup	43
4.5	PWM Generation and Phase Shift Control	44
4.6	Phase Shift Variation Testing	45
4.6.1	Phase Shift = 0.1	46
4.6.2	Phase Shift = 0.2	47
4.6.3	Phase Shift = 0.3	48
4.6.4	Phase Shift = 0.4	50
4.6.5	Discussion: Phase Shift Variation Results	51
4.7	Bidirectional Operation Testing	53
4.7.1	Forward Mode (Charging the Capacitor and Supplying the Load) . .	53
4.7.2	Reverse Mode (Discharging the Supercapacitor and Transferring Power Back to the Input Side)	54
4.7.3	Discussion	54
4.7.4	Efficiency Calculation	54
5	General conclusion	56
Appendices		60

LIST OF FIGURES

1.1	Buck and Boost Derived Bidirectional DC-DC Converter.	3
1.2	Buck-Boost Derived Bidirectional DC-DC Converter.	4
1.3	ĆUK Derived Bidirectional DC-DC Converter.	4
1.4	SEPIC and Zeta Derived Bidirectional DC-DC Converter.	5
1.5	Cascade Bidirectional DC-DC Converter.	5
1.6	Switched-Capacitor Bidirectional DC-DC Converter.	6
1.7	Interleaved Bidirectional DC-DC Converter.	6
1.8	Multilevel Bidirectional DC-DC Converter.	6
1.9	Flyback Bidirectional DC-DC Converter.	7
1.10	Isolated ĆUK Bidirectional DC-DC Converter.	7
1.11	Push-Pull Bidirectional DC-DC Converter.	8
1.12	Forward Bidirectional DC-DC Converter.	8
1.13	Dual Active Bridge Bidirectional DC-DC Converter.	9
1.14	Dual Half-Bridge Bidirectional DC-DC Converter.	9
1.15	Half-Bridge to Full-Bridge Bidirectional DC-DC Converter.	9
1.16	Multiport DAB Bidirectional DC-DC Converter.	10
2.1	General structure of DAB.	15
2.2	Illustration of phase shift between two AC voltage sources representing full-bridge outputs.	16
2.3	DAB Bidirectional DC-DC Converter.	17
2.4	DAB Waveforms.	18
2.5	The primary, secondary sides of the transformer voltage, and the inductor voltage and current waveforms.	19
2.6	Output current or rectified version of inductor current.	19
2.7	Equivalent dab model at high frequencys.	20
2.8	Global DAB diagram.	23

LIST OF FIGURES

3.1 PLECS Model of the DAB Converter	26
3.2 Controller block	27
3.3 PWM Gate Signals for Forward Mode	29
3.4 Waveforms of Primary Voltage, Secondary Voltage, Leakage Inductor Voltage, and Current	30
3.6 Output Current in forward Mode	30
3.5 Output Voltage in forward Mode (48V to 400V)	31
3.7 Power Waveform in forward Mode	31
3.8 PWM Gate Signals for in reverse mode	32
3.9 Waveforms of Primary Voltage, Secondary Voltage, Leakage Inductor Voltage, and Current	33
3.10 Output Voltage in reverse Mode (400V to 48V)	34
3.11 Output Current in reverse Mode	34
3.12 output power waveform in reverse mode	35
4.1 DAB converter diagram	38
4.2 Hardware Implementation of the DAB Converter	38
4.3 Transformer used in DAB converter.	39
4.4 External Leakage Inductance	40
4.5 Primary side voltage waveform	40
4.6 Secondary side voltage waveform	41
4.7 Batteries	41
4.8 Output Load	41
4.9 Supercapacitor 10F	42
4.10 Texas Instruments C2000 MCU	42
4.11 Finirsi 1014D Oscilloscope	43
4.12 Measurement Module	43
4.13 Photograph of the experimental setup	44
4.14 PWM signal for the primary side	44
4.15 PWM signal for the secondary side	45
4.16 Phase shift between primary and secondary PWM signals	45
4.17 PWM Signal at Phase Shift 0.1	46
4.18 Input and Output Current at Phase Shift 0.1	46
4.19 Output Voltage at Phase Shift 0.1	46
4.20 Inductor Current and PWM at Phase Shift 0.1	47
4.21 PWM Signal at Phase Shift 0.2	47
4.22 Input and Output Current at Phase Shift 0.2	47
4.23 Output Voltage at Phase Shift 0.2	48
4.24 Inductor Current and PWM at Phase Shift 0.2	48

LIST OF FIGURES

4.25 PWM Signal at Phase Shift 0.3	48
4.26 Input and Output Current at Phase Shift 0.3	49
4.27 Output Voltage at Phase Shift 0.3	49
4.28 Inductor Current and PWM at Phase Shift 0.3	49
4.29 PWM Signal at Phase Shift 0.4	50
4.30 Input and Output Current at Phase Shift 0.4	50
4.31 Output Voltage at Phase Shift 0.4	50
4.32 Inductor Current and PWM at Phase Shift 0.4	51
4.33 Output Power as a Function of Phase Shift in the DAB Converter	51
4.34 Experimental Setup for Bidirectional Power Transfer in DAB Converter	53
4.35 Output current in forward mode	53
4.36 output current in reverse mode.	54

LIST OF TABLES

1.1	Comparison Between Isolated and Non-Isolated Bidirectional DC-DC Converters	11
1.2	Comparison of Isolated Bidirectional DC-DC Converter Topologies	12
3.1	Simulation Parameters	26
3.2	PI Controller Gains	28
4.1	Measured DAB Parameters at Different Phase Shifts	51

LIST OF ABBREVIATIONS

DAB	Dual Active Bridge
SEPIC	Single-Ended Primary-Inductor Converter
DC	Direct Current
AC	Alternating Current
DSP	Digital Signal Processor
TI	Texas Instruments
SPS	Single Phase Shift
DPS	Dual Phase Shift
MPC	Model Predictive Control
PWM	Pulse Width Modulation
PI	Proportional–Integral
K_p	Proportional Gain
K_i	Integral Gain
PLECS	Piecewise Linear Electrical Circuit Simulation
MOSFET	Metal-Oxide-Semiconductor Field-Effect Transistor
SiC	Silicon Carbide
EE Core	Ferrite Core Standard Type E-E
HV	High Voltage
LV	Low Voltage
FPGA	Field-Programmable Gate Array
ZVS	Zero Voltage Switching
EVs	Electric Vehicles
VM	Voltage Measurement
AM	Current Measurement
LCR Meter	Inductance, Capacitance, and Resistance Meter

LIST OF VARIABLES

L_k	Leakage inductance
V_1	Primary side voltage
V_2	Secondary side voltage
ωL	Angular frequency times inductance
$i(t)$	Instantaneous current
p	Instantaneous power
p_{avg}	Average power
T_s	Switching period
V_{pri}	Primary voltage of transformer
V_{sec}	Secondary voltage of transformer
F_s	Switching frequency
C	Output capacitor
R_l	Load resistance
n	Transformer turns ratio ($n = \frac{N_s}{N_p}$)
D	Duty cycle
N_s	Number of secondary turns
N_p	Number of primary turns

GENERAL INTRODUCTION

The growing demand for efficient, compact, and flexible power conversion solutions is driven by the rapid integration of renewable energy sources, the expansion of energy storage systems, and the rise of electric vehicles. These technologies require power converters capable of bidirectional energy flow and operation across varying voltage levels. Among the available topologies, the Dual Active Bridge (DAB) DC-DC converter stands out due to its high efficiency, galvanic isolation, compact design, and controllable power transfer.

The DAB converter is well-suited for applications that require isolated and efficient energy exchange, such as battery storage, renewable systems, and electric vehicles. Its ability to operate at high frequency helps reduce magnetic component size, while its phase-shift control enables effective power regulation.

However, the design and implementation of DAB converters involve challenges, including control strategy development, transformer design, and performance optimization under variable conditions. This project addresses these challenges by designing, simulating, and experimentally validating a single-phase DAB converter operating between 48V and 400V. Simulations are carried out using PLECS, followed by prototype implementation to confirm system performance.

The project is organized as follows: Chapter 2 presents a literature review. Chapter 3 covers the converter design. Chapter 4 includes simulation results. Chapter 5 describes the hardware implementation, and Chapter 6 concludes the thesis with final remarks and future directions.

CHAPTER 1

LITERATURE REVIEW BIDIRECTIONAL DC-DC CONVERTER

Introduction

Bidirectional DC-DC converters have gained significant attention in power electronics due to their ability to facilitate power flow in both forward and reverse directions. These converters are integral to applications such as electric vehicles (EVs), hybrid electric vehicles (HEVs), renewable energy systems (e.g., photovoltaic and fuel cell systems), and energy storage systems. Unlike unidirectional converters, bidirectional designs eliminate the need for separate converters, enhancing system efficiency and reducing size [1]. The literature categorizes bidirectional DC-DC converters into non-isolated and isolated topologies, providing a comprehensive analysis of their structures, advantages, and applications. The review aims to support the design of a Dual Active Bridge (DAB) converter for a 48 V to 400 V bidirectional DC-DC application, as explored in this project [1].

1.1 Introduction to Bidirectional DC-DC Converters

Bidirectional DC-DC converters (BDC) are power electronic circuits that enable controlled power flow in both directions between two DC voltage levels. Unlike unidirectional converters that only allow energy transfer from input to output, bidirectional converters can reverse the direction of power flow depending on system requirements. This capability is essential in applications involving energy storage, regenerative braking, and renewable energy systems where energy may need to be both absorbed and delivered.

Before discussing specific converter topologies, bidirectional DC-DC converters can generally be divided into two main categories: isolated and non-isolated. Non-isolated topologies are typically used for lower voltage applications where galvanic isolation is not required, of-

ferring simpler design and higher efficiency. Isolated topologies, on the other hand, provide electrical isolation between input and output, which is essential for safety, higher voltage levels, and certain industrial and grid-connected applications [2].

1.2 Non-Isolated Bidirectional DC-DC Converter Topologies

Non-isolated DC-DC converters transfer power without electrical isolation between input and output. They are simple, efficient, and commonly used in low-voltage applications like mobile devices and power supplies, but are unsuitable for systems requiring safety isolation

1.2.1 Buck and Boost Derived Topology

This topology is derived from buck and boost converters by replacing unidirectional switches with bidirectional power switches. It operates in boost mode from a low voltage (V_L) to a high voltage (V_H) and buck mode from V_H to V_L , offering a simple configuration without magnetic isolation. It is best suited for low-power applications such as small-scale energy storage systems or auxiliary power supplies in EVs [2].

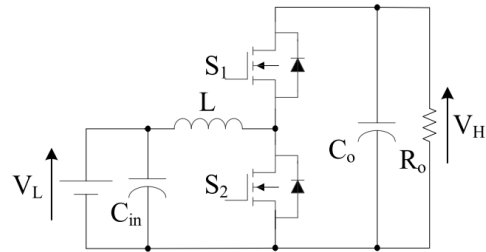


Figure 1.1: Buck and Boost Derived Bidirectional DC-DC Converter [1].

1.2.2 Buck-Boost Derived Topology

The buck-boost topology is created by substituting unidirectional switches with bidirectional ones, enabling power flow in both directions with the capability to buck or boost negative voltage levels. Its flexibility in voltage regulation makes it ideal for battery management systems in EVs or renewable energy integration where variable voltage levels are required [3].

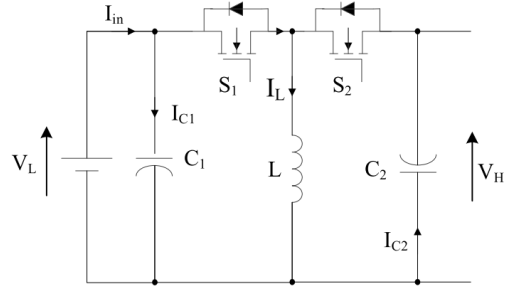


Figure 1.2: Buck-Boost Derived Bidirectional DC-DC Converter [1].

1.2.3 ĆUK Derived Topology

The ĆUK topology ensures continuity of input current and output voltage by using two bidirectional switches and a coupled inductor to minimize current ripple. This feature makes it suitable for applications sensitive to current disturbances, such as renewable energy systems with photovoltaic panels or fuel cells [4].

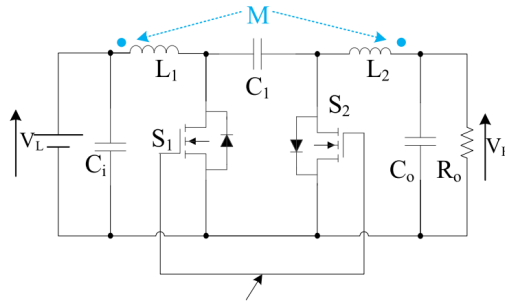


Figure 1.3: ĆUK Derived Bidirectional DC-DC Converter [1].

1.2.4 SEPIC and Zeta Derived Topology

By rearranging ĆUK elements, SEPIC and Zeta converters provide a positive voltage output, functioning as Zeta in high-to-low voltage mode and SEPIC in low-to-high voltage mode. This versatility is advantageous for hybrid energy systems or EV charging stations requiring adaptive voltage conversion [3].

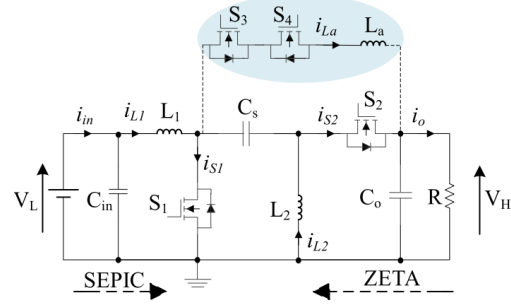


Figure 1.4: SEPIC and Zeta Derived Bidirectional DC-DC Converter [1].

1.2.5 Cascade Topology

This topology connects two buck-boost converters back-to-back, reducing output current stress and boosting voltage. It is commonly used in EV systems for high-efficiency power transfer, though it increases the number of passive components, making it suitable for medium-power applications [5].

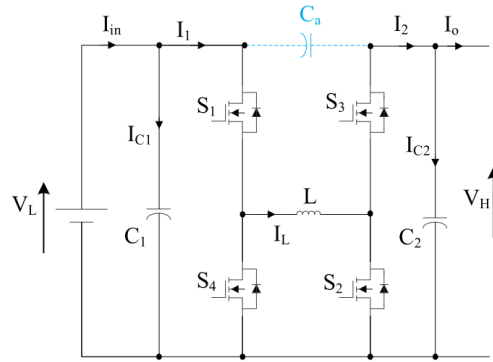


Figure 1.5: Cascade Bidirectional DC-DC Converter [1].

1.2.6 Switched-Capacitor Topology

Utilizing switched-capacitors, this topology enhances voltage boosting and reduces weight [6], achieving continuous current. It is ideal for compact, lightweight applications like portable energy storage devices, despite introducing switching frequency current ripple [1].

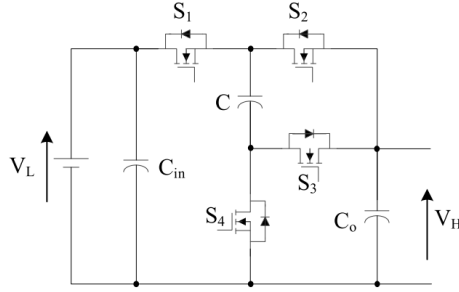


Figure 1.6: Switched-Capacitor Bidirectional DC-DC Converter [1].

1.2.7 Interleaved Topology

The interleaved technique eliminates switching frequency current ripple and electromagnetic interference [7], improving transient response by varying switch patterns. It is well-suited for high-current applications such as EV battery chargers or grid-tied renewable systems.

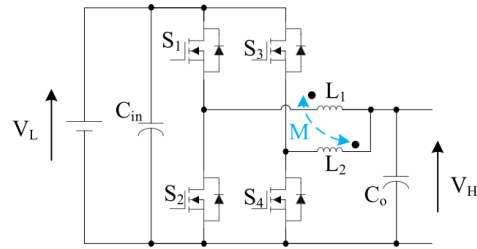


Figure 1.7: Interleaved Bidirectional DC-DC Converter [1].

1.2.8 Multilevel Topology

Employing two voltage bridges without inductors, this topology achieves high voltage gain and low weight. It is primarily used in EV battery charging applications or high-voltage DC systems requiring efficient power delivery [2].

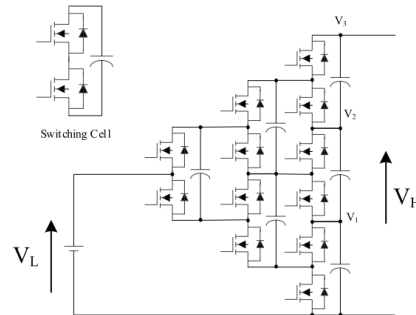


Figure 1.8: Multilevel Bidirectional DC-DC Converter [1].

1.3 Isolated Bidirectional DC-DC Converter Topologies

1.3.1 Flyback Topology

The Flyback converter, derived from a buck-boost with a transformer, provides magnetic isolation and high voltage gain based on the transformer turns ratio (N). It is suitable for low-to-medium power applications like auxiliary power supplies or small-scale energy storage [8].

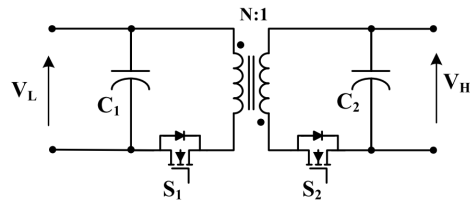


Figure 1.9: Flyback Bidirectional DC-DC Converter [1].

1.3.2 Isolated ĆUK Topology

This isolated version of the ĆUK converter offers continuous input/output current and high voltage gain, enhanced by a coupled inductor to reduce ripple. It is recommended for renewable energy systems like solar or wind power integration [2].

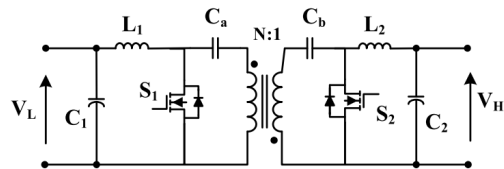


Figure 1.10: Isolated ĆUK Bidirectional DC-DC Converter [1].

1.3.3 Push-Pull Topology

Using a multi-winding transformer, the push-pull topology enables bidirectional power flow [9], making it suitable for medium-power applications such as uninterruptible power supplies (UPS) or industrial power systems.

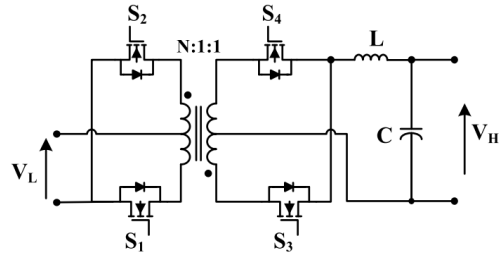


Figure 1.11: Push-Pull Bidirectional DC-DC Converter [1].

1.3.4 Forward Topology

The forward topology, with a clamped circuit for zero voltage switching, leverages transformer leakage inductance for resonant operation. It is ideal for applications requiring soft-switching, such as EV auxiliary systems [9].

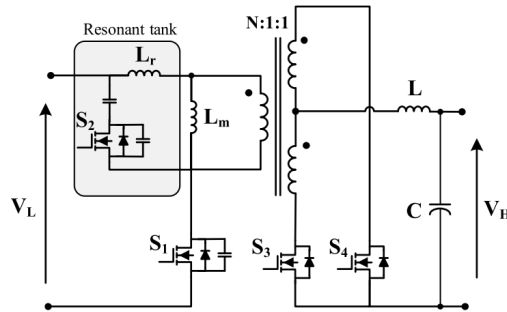


Figure 1.12: Forward Bidirectional DC-DC Converter [1].

1.3.5 Dual Active Bridge (DAB) Topology

The DAB topology employs two full-bridge circuits with a high-frequency transformer, offering high voltage gain and galvanic isolation. It is ideal for high-power applications like the proposed 48 V to 400 V DAB converter in EVs or grid-connected energy storage systems, with power regulated by phase-shift control [10].

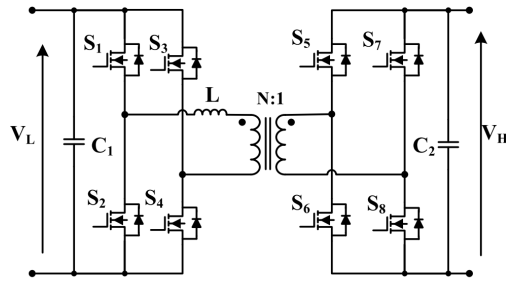


Figure 1.13: Dual Active Bridge Bidirectional DC-DC Converter [1].

1.3.6 Dual Half-Bridge Topology

With four switches and no right half-plane zero, this topology simplifies controller design and suits lower-power applications like residential energy storage or small EV systems [2].

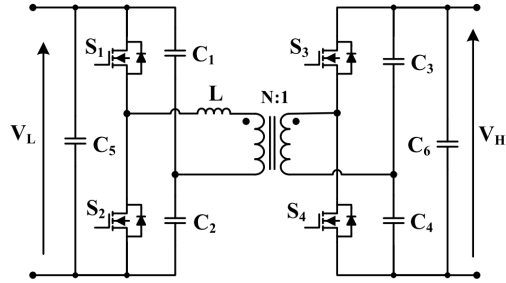


Figure 1.14: Dual Half-Bridge Bidirectional DC-DC Converter [1].

1.3.7 Half-Bridge to Full-Bridge Topology

This configuration uses a half-bridge on the primary and a full-bridge on the secondary, reducing switch count and control complexity. It is well-suited for UPS systems or hybrid energy setups [2].

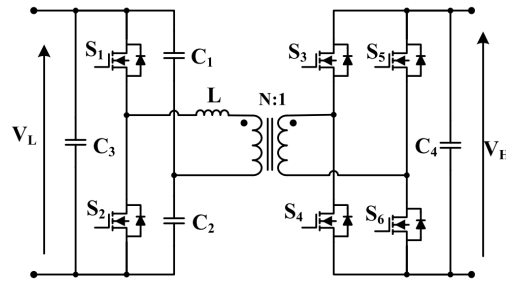


Figure 1.15: Half-Bridge to Full-Bridge Bidirectional DC-DC Converter [1].

1.3.8 Multiport DAB Topology

Designed for multi-input systems, this topology uses a multi-winding transformer [11] to manage power flow from multiple sources. It is optimal for renewable energy integration or hybrid EV systems with diverse energy inputs.

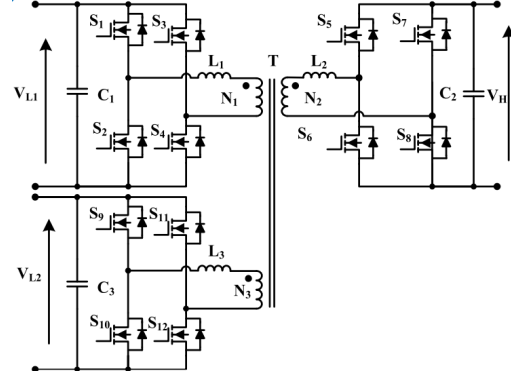


Figure 1.16: Multiport DAB Bidirectional DC-DC Converter [1].

1.4 Comparison Between Isolated and Non-Isolated Bidirectional DC-DC Converters

Bidirectional DC-DC converters can be broadly classified into isolated and non-isolated types. Non-isolated converters are generally simpler, more compact, and cost-effective, making them suitable for low-power applications where galvanic isolation is not required. In contrast, isolated converters provide electrical isolation between input and output, which enhances safety and allows operation over a wider voltage range. This makes them ideal for high-power applications such as electric vehicles, energy storage systems, and grid-connected converters, despite their higher complexity and cost [1, 2, 7].

Table 1.1: Comparison Between Isolated and Non-Isolated Bidirectional DC-DC Converters

Criteria	Non-Isolated Converters	Isolated Converters
Galvanic Isolation	No isolation between input and output	Provides electrical isolation
Complexity	Simple circuit topology	More complex (transformer + control)
Cost	Lower cost (fewer components)	Higher cost (transformer, more switches)
Size	Smaller size for low-power systems	Bulkier due to transformer (unless using HF transformers)
Safety	Less safe (risk of ground faults)	Safer (isolation protects users and equipment)
Efficiency	High at low power levels	High at medium-to-high power levels
Voltage Range	Limited input/output voltage difference	Large voltage step-up or step-down possible
Control Complexity	Simpler control	More complex (phase-shifted control, transformer magnetics)
Typical Applications	Battery management systems, small ESS, portable devices	EVs, grid storage, fast chargers, industrial systems

1.5 Comparison Between Isolated Bidirectional DC-DC Converter Topologies

Several isolated bidirectional DC-DC converter topologies exist, each with distinct advantages and limitations. The Dual Active Bridge (DAB) converter is widely used for high-power applications due to its soft-switching capability and high efficiency, but requires complex control strategies. Flyback and forward converters are simpler and cost-effective for low-to-medium power levels, though flyback suffers from higher voltage stresses. Push-pull converters offer better transformer utilization but are generally limited to lower voltage applications. Resonant and LLC converters provide excellent efficiency and high-frequency operation, making them suitable for compact, high-density power supplies despite their design complexity [2].

Table 1.2: Comparison of Isolated Bidirectional DC-DC Converter Topologies

Topology	Advantages	Disadvantages	Typical Applications
Dual Active Bridge (DAB)	High power density, soft switching (ZVS), wide voltage range, bidirectional operation	Complex control (phase-shift), sensitive to transformer leakage inductance	EV chargers, energy storage systems, grid interface
Bidirectional Flyback	Simple, low cost, few components, compact design	High voltage stress, limited power capacity, hard switching	Portable devices, low-power backup systems, UPS
Bidirectional Forward	Higher efficiency than flyback, simple transformer design, suitable for medium power	Limited to moderate power levels, requires demagnetizing circuit	Telecom power supplies, industrial converters
Bidirectional Push-Pull	Simple transformer design, better transformer utilization, easy current sharing	High voltage stress on switches, not suitable for high voltage	DC microgrids, battery chargers
Resonant/LLC	High efficiency, soft switching across wide load range, high-frequency operation	Complex control, sensitive to load variations, difficult design	Server power supplies, datacenters, aerospace converters

1.6 Why the Dual Active Bridge is a Preferred Topology

Among isolated bidirectional DC-DC converters, the Dual Active Bridge (DAB) topology is widely preferred for medium to high-power applications. This is due to its ability to achieve high efficiency through soft-switching (Zero Voltage Switching - ZVS), which reduces switching losses at high frequencies. The DAB also allows bidirectional power flow with simple phase-shift control, making it highly flexible for various applications. Additionally, the presence of galvanic isolation ensures safety and compliance with grid and industrial standards. Its modular structure, scalability, and compatibility with modern wide-bandgap semiconductor devices further enhance its attractiveness in electric vehicles, renewable energy systems, and grid-connected storage applications [2, 10].

1.7 Control Strategies for Bidirectional DC-DC Converters

Bidirectional DC-DC converters play a central role in modern power electronics systems, such as renewable energy interfaces, electric vehicles, and battery storage. Their ability to transfer energy in both directions—typically from a low-voltage to a high-voltage domain and vice versa—necessitates a control system that is both precise and adaptive.

1.7.1 Single Phase Shift (SPS) Control

In this work, the initial control strategy implemented was the Single Phase Shift (SPS) method, which is widely used for Dual Active Bridge (DAB) converters due to its simplicity and ease of implementation [12]. The SPS technique controls the power flow by varying the phase shift between the primary and secondary bridge switching signals. The amount of transferred power is proportional to the sine of the phase difference, making this method suitable for steady-state operation and symmetrical conditions [13].

SPS provides a straightforward way to achieve zero-voltage switching (ZVS) and is highly compatible with digital controllers such as the TI C2000 series. However, SPS may result in low efficiency under light load or asymmetrical conditions, where current stress increases.

1.7.2 Alternative Control Strategies

While SPS is effective, several advanced control techniques have been proposed to address its limitations:

- **Dual Phase Shift (DPS):** Unlike SPS, DPS introduces an additional degree of freedom by allowing independent phase shifts on both the leading and lagging edges of the bridge switches. This enables better control over circulating current and improves efficiency under variable load conditions [14].
- **Triple Phase Shift (TPS):** This method provides even more flexibility by controlling the phase shifts within each bridge leg independently. TPS can further optimize power flow and reduce current stress, though it increases control complexity [14].
- **Model Predictive Control (MPC):** MPC offers a predictive, optimization-based approach that can handle system constraints and nonlinearities. It provides excellent dynamic response and minimal steady-state error, but requires high computational resources, making it more suitable for high-performance applications [15].
- **Hysteresis Control:** Based on switching when current or voltage crosses defined thresholds. This method is simple and fast but can result in variable switching frequency, which complicates filter design [16].

- **Current Mode Control (CMC):** Uses the inductor current as a feedback signal for improved dynamic response and current limiting. Often used in battery charging/discharging applications [16].
- **Artificial Intelligence-based Control:** Recently, fuzzy logic and neural network controllers have been proposed for adaptive real-time optimization, especially in renewable energy systems. However, these methods are still under development for practical deployment [17].

Each method presents trade-offs in complexity, hardware requirements, efficiency, and dynamic response. The choice of control strategy depends on the application requirements, such as load dynamics, system cost, and control precision.

In this project, the SPS method was selected for its simplicity, compatibility with the hardware platform (TI C2000), and suitability for initial validation of bidirectional energy transfer.

Conclusion

This chapter has presented a comprehensive review of bidirectional DC-DC converters with a particular focus on the Dual Active Bridge (DAB) topology. A analysis of various control strategies was also conducted. Among these, the Single Phase Shift (SPS) control method stands out for its simplicity and ease of implementation, particularly in real-time digital control environments.

The insights gained from the literature provide a strong foundation for the subsequent chapters, where the focus will shift to the practical system design and implementation of a DAB converter.

CHAPTER 2

DAB CONVERTER SYSTEM DESIGN

Introduction

This chapter presents the system design of the Dual Active Bridge (DAB) converter, covering its overall architecture, power stage configuration, control strategy, and key component selection. The goal is to define a practical and efficient design framework that ensures reliable bidirectional power transfer, supports the intended application requirements, and lays the foundation for hardware implementation and control development.

2.1 System Overview

The DAB converter consists of two full-bridge inverters connected through a high-frequency transformer with a leakage inductance L_k . The converter enables bidirectional power transfer controlled through phase-shift modulation between the primary and secondary bridge switching signals.

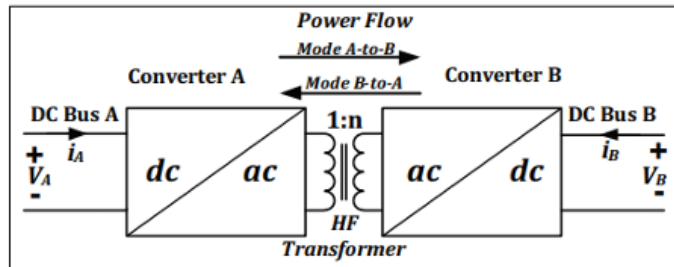


Figure 2.1: General structure of DAB [18].

2.2 Dual Active Bridge Analogy With Power Systems

The operation of a Dual Active Bridge (DAB) converter can be understood through an analysis of power flow between two alternating voltage waveforms. Since the transformer in a DAB topology transfers energy in AC form, each side of the converter produces a square-wave AC voltage from its respective DC input using a full-bridge inverter. The energy transfer occurs through the high-frequency transformer based on the phase difference between these two AC waveforms.

By introducing a controllable phase shift between the primary and secondary full-bridge converters, the direction and magnitude of power flow can be precisely regulated. This principle is commonly represented by two phase-shifted square-wave voltage sources, where V_1 and V_2 denote the amplitudes and θ_1 , θ_2 their respective phase angles [11].

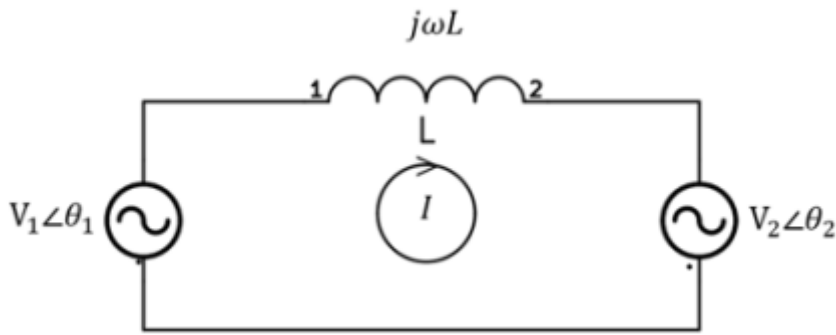


Figure 2.2: Illustration of phase shift between two AC voltage sources representing full-bridge outputs [18].

Initially, the reference phase angle of the primary-side voltage source is set to $\theta_1 = 0$, while the secondary-side voltage source has a relative phase angle θ_2 . The resulting loop current through the leakage inductance can be described in phasor form as:

$$\vec{I} = \frac{\vec{V}_1 - \vec{V}_2}{j\omega L} = \frac{V_1 \angle 0^\circ - V_2 \angle \theta_2}{j\omega L} \quad (2.1)$$

The above equation can be represented in the time domain.

$$v_1(t) = V_1 \sin(\omega t), \quad v_2(t) = V_2 \sin(\omega t - \theta_2)$$

So,

$$I(t) = \frac{V_1}{\omega L} \sin(\omega t) - \frac{V_2}{\omega L} \sin(\omega t - \theta_2) \quad (2.2)$$

The value $I(t)$ from the equation above can be used to express the power on the secondary side.

$$p_2(t) = v_2(t) \cdot i(t) = \frac{V_2}{\omega L} \sin(\omega t - \theta_2) [V_1 \sin(\omega t) - V_2 \sin(\omega t - \theta_2)] \quad (2.3)$$

The average power throughout one period can be denoted as T_s , resulting in more straight-

forward equations.

$$P_{2,\text{avg}} = \frac{1}{T_s} \int_0^{T_s} p_2(t) dt \quad (2.4)$$

After putting equation 2.3 in 2.4 and integrating it leads to equation 2.5

$$P_2 = \frac{V_1 V_2}{\omega L} \sin(\theta_2) \quad (2.5)$$

The equation above describes the principle of power transfer in a Dual Active Bridge (DAB) converter, where the phase angle θ_2 directly controls the direction and magnitude of energy flow. When θ_2 is positive, power flows from the primary side (V_1) to the secondary side (V_2). Conversely, a negative θ_2 results in power flowing from V_2 back to V_1 .

This method of phase-shift-based control relies on the presence of an inductive element to facilitate energy transfer. In the DAB converter, the transformer's leakage inductance fulfills this role. Although the converter operates using square-wave voltage signals rather than ideal sine waves, the fundamental power transfer behavior remains governed by the same physical principles.

2.3 Fundamental Working of the DAB Converter

In the Dual Active Bridge (DAB) converter, the primary-side full-bridge operates as an inverter, while the secondary-side bridge functions as a rectifier. Power transfer is governed by the phase shift between the switching signals applied to each bridge, as previously discussed. Phase-shifted PWM control signals are used to modulate both the primary and secondary bridges, as illustrated in Figure 2.3.

Each full-bridge consists of two complementary switch pairs. These pairs are driven alternately, operating at the same switching frequency with a 50% duty cycle. A small dead time is introduced between transitions to prevent shoot-through, and the switching pattern is repeated every switching period T_s .

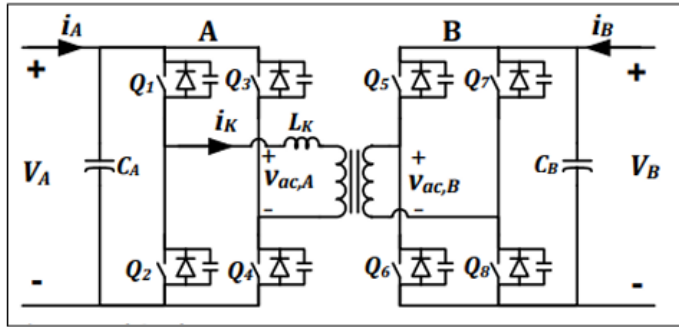


Figure 2.3: DAB Bidirectional DC-DC Converter [18].

The current flowing through the transformer's leakage inductance governs the power transfer in the Dual Active Bridge (DAB) converter. This current is influenced by the

primary and secondary side voltages (V_{prim} and V_{sec}), the leakage inductance L_k , and the phase shift between the switching signals, as described in Equation 2.5.

The inductor current is directly related to the voltage applied across it and its inductance, as outlined in Equations 2.6 and 2.7. The voltage across the leakage inductance itself is defined as the instantaneous difference between the voltages on the primary and secondary sides of the transformer. Over one switching period, this voltage waveform is typically divided into four distinct intervals for analysis.

$$L_k \frac{di_L(t)}{dt} = v_L(t) \quad (2.6)$$

$$v_L(t) = v_1(t) - v_2(t) \quad \text{where } 0 < t < \frac{T_s}{2} \quad (2.7)$$

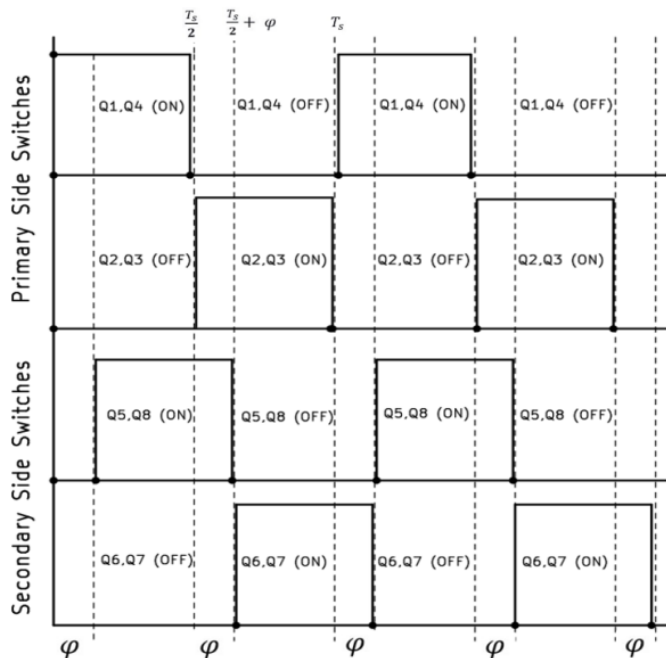


Figure 2.4: DAB Waveforms [18].

Under ideal operating conditions (neglecting losses), the primary-side switches Q_1 and Q_4 are turned on during the first half of the switching period $T_s/2$, resulting in $V_{\text{prim}} = V_{\text{in}}$. In the second half, switches Q_2 and Q_3 are turned on, giving $V_{\text{prim}} = -V_{\text{in}}$.

On the secondary side, a phase shift ϕ is introduced. Switches Q_8 and Q_5 conduct from $T_s/2$ to $T_s/2 + \phi$, while switches Q_6 and Q_7 are active from $T_s/2 + \phi$ to $T_s + \phi$.

The voltage across the leakage inductance is the difference between the primary and secondary voltages of the transformer. This voltage drives the inductor current, which forms a trapezoidal waveform with a zero average over one switching cycle, as illustrated in Figure 2.5. Since the secondary bridge functions as a rectifier, the output current is a rectified version of the inductor current, shown in Figure 2.6.

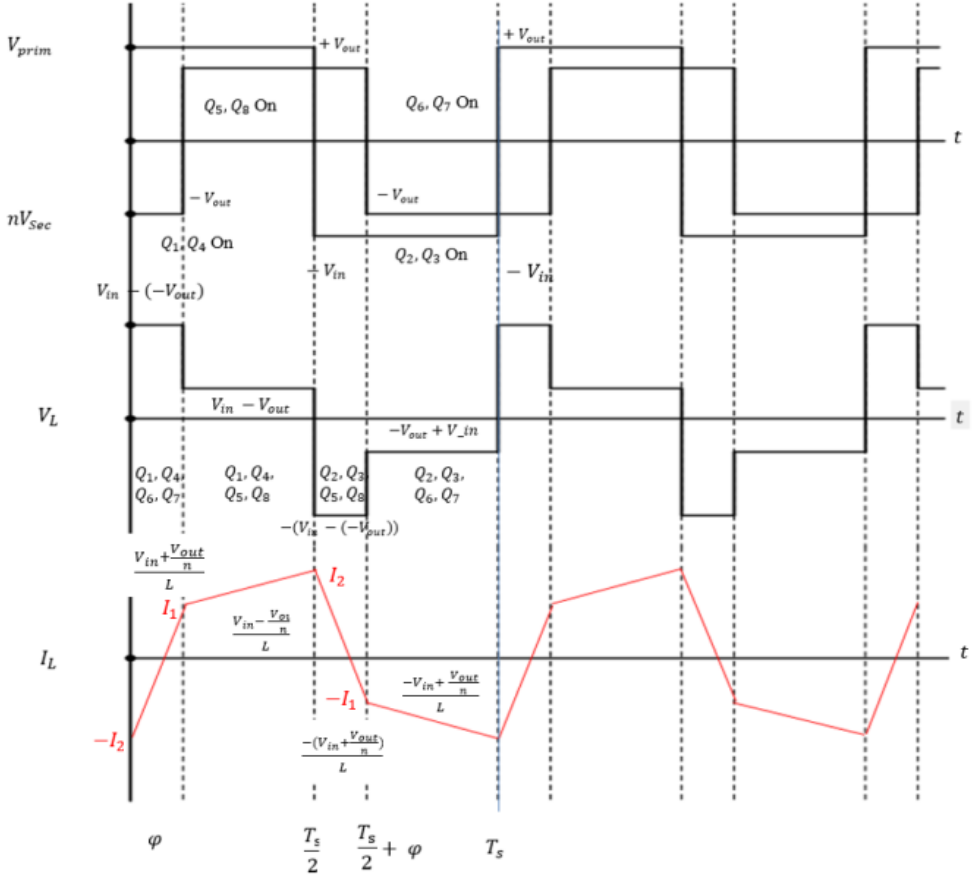


Figure 2.5: The primary, secondary sides of the transformer voltage, and the inductor voltage and current waveforms [18].

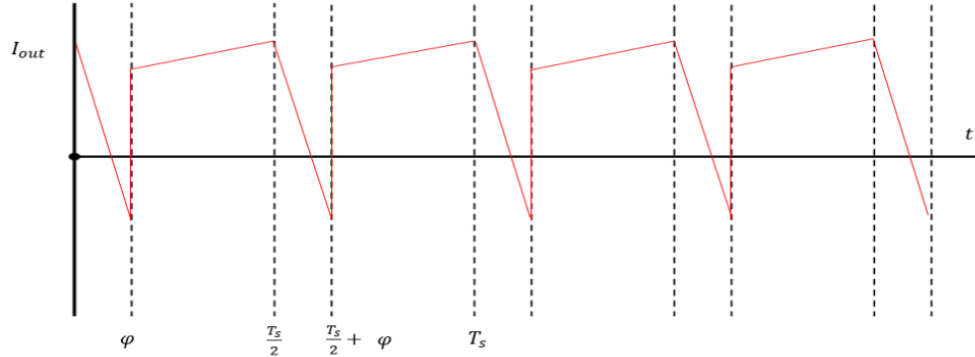


Figure 2.6: Output current or rectified version of inductor current [18].

The average output current can be calculated by integrating the inductor current over half of the switching period. This leads to the following expression:

$$I_{\text{out}} = \frac{V_{\text{in}}}{2nL_k f_{\text{sw}}} D(1 - D) \quad (2.8)$$

where $D = \frac{\varphi}{T_s/2}$ is the normalized phase shift, and $-0.5 \leq D \leq 0.5$.

Similarly, the output power can be determined from the product of output current and secondary voltage:

$$P_{\text{out}} = \frac{V_{\text{in}} \cdot V_{\text{out}}}{2nL_k f_{\text{sw}}} D(1 - D) \quad (2.9)$$

The given expression describes the relationship between output power and factors such as the duty cycle of the primary and secondary side bridges, leakage inductance (which facilitates energy transfer), and the converter's switching frequency. Conversely, a negative duty cycle or phase shift can lead to reverse power flow from the secondary side to the primary side.

2.4 Transformer Design and Leakage Inductance Considerations

To meet design requirements, high-frequency switching is utilized, which minimizes the size of passive components. At high frequencies, the magnetizing inductance becomes negligible, allowing the transformer to be modeled solely with a leakage inductor, which acts as the energy inductor in a dual active bridge. If the leakage inductance is inadequate for energy transfer, an additional inductor can be connected in series with the transformer. A high-frequency equivalent model of the dual active bridge, incorporating the leakage inductor, is depicted in Figure 2.7.

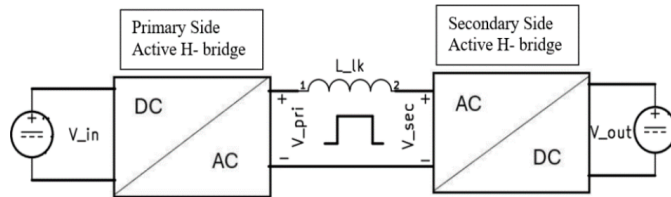


Figure 2.7: Equivalent dab model at high frequencies [18].

Figure 2.7 illustrates an equivalent model of a dual active bridge under operating conditions, comprising a primary side active H-bridge and a secondary side active H-bridge. These bridges generate two complementary high-frequency AC square waves, which can be phase-shifted relative to each other. The resulting AC square wave produces a voltage difference across the leakage inductance, which serves as the energy transfer inductor. To meet the power requirements, a high-frequency transformer with a turn ratio of $n = 8.333$ was selected, optimized for a 48V input voltage, a 400V output voltage, and a 4kW power rating.

$$n = \frac{N_s}{N_p} = 8.33 \quad (2.10)$$

where n is the secondary to primary turns ratio. With:

$$\frac{V_2}{V_1} = n, \quad \frac{I_2}{I_1} = \frac{1}{n}$$

To determine the required leakage inductance for the proposed converter, Equation 2.11 is used. This expression is a rearranged form of the output power equation 2.9, solving for L_k . Based on the converter's design parameters, the required leakage inductance is calculated to be approximately 720 nH.

$$L_k = \frac{V_{\text{in}} \cdot V_{\text{out}}}{2n P_{\text{out}} f_{\text{sw}}} D(1 - D) = 720 \text{ nH} \quad (2.11)$$

where,

- $V_{\text{in}} = 48 \text{ V}$: Input voltage on the primary side.
- $V_{\text{out}} = 400 \text{ V}$: Output voltage on the secondary side.
- $n = 8.33$: Transformer turns ratio, defined as $n = \frac{N_{\text{sec}}}{N_{\text{prim}}}$.
- $f_{\text{sw}} = 100 \text{ kHz}$: Switching frequency of the converter.
- $P_{\text{out}} = 4000 \text{ W}$: Rated output power.
- $D = 0.5$: Normalized phase shift at maximum power transfer, defined as $D = \frac{\phi}{T_s/2}$, where ϕ is the phase shift duration.

2.5 Output Capacitor Selection

The output capacitor in the Dual Active Bridge (DAB) converter plays a vital role in filtering the rectified inductor current and maintaining a stable output voltage with minimal ripple. The required capacitance can be estimated based on the desired voltage ripple and the charge transferred per switching cycle.

Assuming a triangular ripple current, the minimum output capacitance C can be calculated using:

$$C_{\text{out}} = \frac{Q}{2 \cdot \Delta V} \quad (2.12)$$

Where:

- Q : Charge transferred during one switching cycle (Coulombs),
- ΔV : Allowable output voltage ripple (Volts).

The value of Q can be derived from the output current ripple, which depends on system parameters such as switching frequency, inductance, duty ratio, and voltage levels. Once Q is known, equation (2.12) is used to determine the required capacitor value.

2.6 Control System

The control system of a Dual Active Bridge (DAB) converter plays a critical role in ensuring accurate power flow regulation, Zero Voltage Switching (ZVS), and output voltage stabilization under dynamic conditions. Figure 2.8 illustrates the overall control system architecture typically used in DAB applications, consisting of cascaded voltage and current PI controllers, with a modulation block generating phase-shift-based PWM signals for the primary (inverter) and secondary (rectifier) full bridge [19].

2.6.1 Dynamic Modeling and Control

To develop a reliable control strategy, it is essential to understand the dynamic behavior of the DAB converter. This is achieved by linearizing the power flow equations around a specific operating point to derive small-signal models. These models help predict the system's frequency response and assist in the design of stable controllers.

The dynamics of the output filter capacitor C_2 and the load resistance R_L are taken into account, while the dual-bridge converter is modeled as a controllable power source. we have:

$$C_{out} \frac{dv_{out}(t)}{dt} = \frac{P_{out}}{V_{out}} - \frac{v_{out}(t)}{R_L} \quad (2.13)$$

By substituting the expression for P_{out} from Equation (1.8) into the output voltage dynamic equation, we obtain:

$$C_{out} \frac{dv_{out}(t)}{dt} = \frac{V_{in} V_{out} \delta(t) [\pi - \delta(t)]}{\omega L_k \pi n} - \frac{v_{out}(t)}{R_L} \quad (2.14)$$

The nonlinearity in Equation (3.14) arises from the fact that both $v_2(t)$ and $\delta(t)$ are time-varying signals. To facilitate control system design, this equation is linearized, leading to the small-signal representation expressed in Equation (3.17).

$$C_{out} \frac{d\tilde{v}_{out}}{dt} = \left. \frac{\partial f}{\partial \delta} \right|_{\delta_s, \tilde{v}_{out}} \delta + \left. \frac{\partial f}{\partial \tilde{v}_{out}} \right|_{\delta_s, \tilde{v}_{out}} \tilde{v}_{out} \quad (2.15)$$

$$C_{out} \frac{d\tilde{v}_{out}(t)}{dt} = \frac{V_{in}}{n \omega L} \left(1 - \frac{2\delta}{\pi} \right) \delta(t) - \frac{1}{R_L} \tilde{v}_{out}(t) \quad (2.16)$$

The variables $\delta(t)$ and $v_{out}(t)$ denote the time-dependent small-signal perturbations of the phase shift and the output voltage, respectively, around a steady-state operating point defined by the nominal phase shift δ . By applying Laplace transformation to the linearized dynamic equation, the system behavior can be expressed in the frequency domain through the transfer function, as presented in Equation (3.17).

$$G_{vd}(s) = \frac{\left(\frac{V_{in}R_L(1-\frac{2\delta}{\pi})}{2\pi f L_k n}\right)}{RCs + 1} \quad (2.17)$$

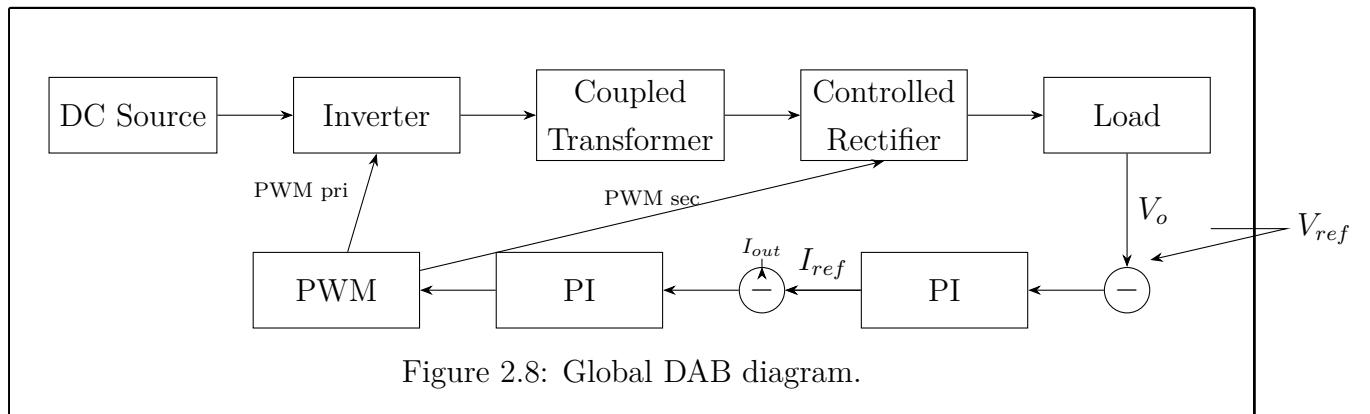
This represents a first-order system with a time constant RC , and it captures the effect of phase shift variations on the output voltage. Such a model is essential for designing inner current and outer voltage control loops.

2.6.2 Control Architecture

The DAB converter uses a dual-loop control structure:

- The outer voltage control loop regulates the output voltage V_o by comparing it to the reference V_{ref} and generates the reference output current.
- The inner current control loop compares the actual output current I_o with the reference, adjusting the phase shift through a PI controller to regulate power flow.

This architecture allows fast dynamic response and better decoupling of voltage and current control. The output of the inner controller is a phase shift command, which is sent to a modulation block that generates complementary PWM signals for both bridges.



2.7 Losses in DAB Converter

The total losses in the DAB converter can be categorized as:

- **Conduction losses:** Due to semiconductor ON-resistance and transformer winding resistance.
- **Switching losses:** Due to finite switching speed of power devices.
- **Core losses:** Due to hysteresis and eddy currents in the transformer core.
- **Leakage inductance losses:** Resulting from circulating current due to imperfect phase-shift control.

Conclusion

This chapter presented the system-level design of the Dual Active Bridge converter, including architecture, power flow, key equations, transformer modeling, and component sizing. These form the basis for control and hardware implementation in subsequent chapters.

CHAPTER 3

SIMULATION

Introduction

This chapter presents the simulation of the designed Dual Active Bridge (DAB) bidirectional DC-DC converter system. The primary objective of the simulation is to validate the theoretical design, evaluate the performance of the control strategy, and observe key electrical waveforms under different operating modes.

3.1 Objectives of the Simulation

The purpose of this simulation is to validate the design of a Dual Active Bridge (DAB) bidirectional DC-DC converter using simulation tools. This includes verifying voltage levels, current waveforms, power transfer efficiency, and control performance under various operating conditions.

3.2 Simulation Tools Used

The simulation was carried out using **PLECS**, a specialized tool for modeling and simulating power electronics systems. PLECS is preferred for its accuracy in simulating switching behavior, ease of integrating control blocks, and real-time simulation capabilities.

3.3 System Parameters

The following table summarizes the main parameters used in the simulation:

Parameter	Value
Input Voltage (V_{in})	48 V
Output Voltage (V_{out})	400 V
Rated Power	4 kW
Switching Frequency (f_s)	100 kHz
Transformer Turns Ratio (n)	8.33
Leakage Inductance (L)	0.72 μ H
Filter Capacitance (C)	1400 μ F
Load Resistance (R)	1 Ω

Table 3.1: Simulation Parameters

3.4 Simulation Model Overview

Figure 3.1 shows the schematic of the DAB converter implemented in PLECS. The model includes two full-bridge converters connected through a high-frequency transformer, along with input and output filters.

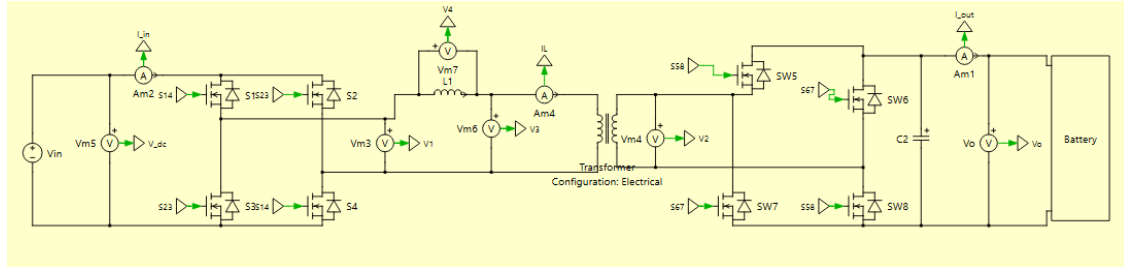


Figure 3.1: PLECS Model of the DAB Converter

3.5 Controller Design and Implementation

The dual active bridge converter is controlled using a phase-shift modulation strategy to regulate power flow between the input and output. The controller adjusts the phase shift angle between the primary and secondary bridges based on the output voltage feedback to maintain the desired voltage level.

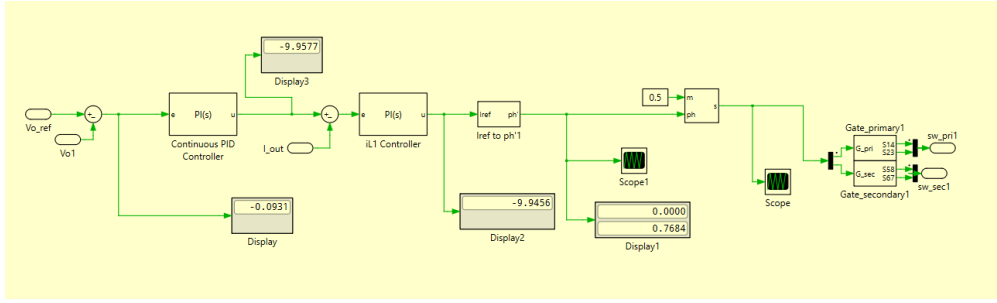


Figure 3.2: Controller block

Figure 3.2 shows the control block diagram implemented in the simulation. The output voltage is measured and compared with the reference voltage, generating an error signal that feeds a PI controller. The controller output determines the phase shift angle, which modulates the PWM signals driving the converter switches.

3.6 Phase Shift Calculation

To regulate the power transfer, the controller calculates the phase shift ϕ from the output of the current controller I_{ref} . The relationship used is derived from the power transfer function of a Dual Active Bridge:

$$\phi = \frac{\pi}{2} \left(1 - \sqrt{1 - \frac{8fL_k|I_{\text{ref}}|}{nV_{in}}} \right) \quad (3.1)$$

- f : Switching frequency (100 kHz)
- L_k : Leakage or interfacing inductance
- n : Transformer turns ratio
- V_{in} : Input-side DC voltage

The expression is implemented using a function block in PLECS. It includes logic for handling negative I_{ref} , ensuring the resulting ϕ drives power in the appropriate direction.

The calculated ϕ is then used to generate the gate signals for the primary and secondary bridges via phase-shift modulation.

3.7 Control System Description

The control structure consists of two cascaded loops:

- **Outer voltage loop:** Generates a current reference I_{ref} by comparing the output voltage V_o with the reference voltage $V_{o,\text{ref}}$.

- **Inner current loop:** Regulates the inductor current I_L by adjusting the phase shift angle ϕ of the DAB converter.

3.7.1 Voltage Loop Equation

$$e_v(t) = V_{o,\text{ref}}(t) - V_o(t)$$

$$I_{\text{ref}}(t) = K_{pv} \cdot e_v(t) + K_{iv} \int e_v(t) dt$$

3.7.2 Current Loop Equation

$$e_i(t) = I_{\text{ref}}(t) - I_{\text{out}}(t)$$

$$\phi(t) = K_{pi} \cdot e_i(t) + K_{ii} \int e_i(t) dt$$

3.7.3 PI Controller Gains

The following table lists the PI gain values used in the simulation:

Table 3.2: PI Controller Gains

Controller	K_p	K_i
Voltage PI (Outer Loop)	0.1	0.5
Current PI (Inner Loop)	0.0531	3.5

The controller parameters were tuned using the SISO Tool in MATLAB to achieve stable operation with minimal overshoot and low steady-state error. The effectiveness of the designed controller is validated through the stable output voltage and power waveforms observed during simulation.

3.8 Simulation Scenarios and Results

3.8.1 Steady-State Operation

The converter was simulated in both power flow directions: forward mode (48V to 400V) and reverse mode (400V to 48V). In each case, key waveforms were recorded and analyzed.

Stage 1: forward Mode (Low to High Voltage)

In this stage, the converter transfers power from 48V (low voltage side) to 400V (high voltage side). The following waveforms were obtained: Figure 3.4 illustrates the waveforms of primary voltage (V_{m3}), secondary voltage (V_{m4}), inductor voltage (V_{m7}), and inductor

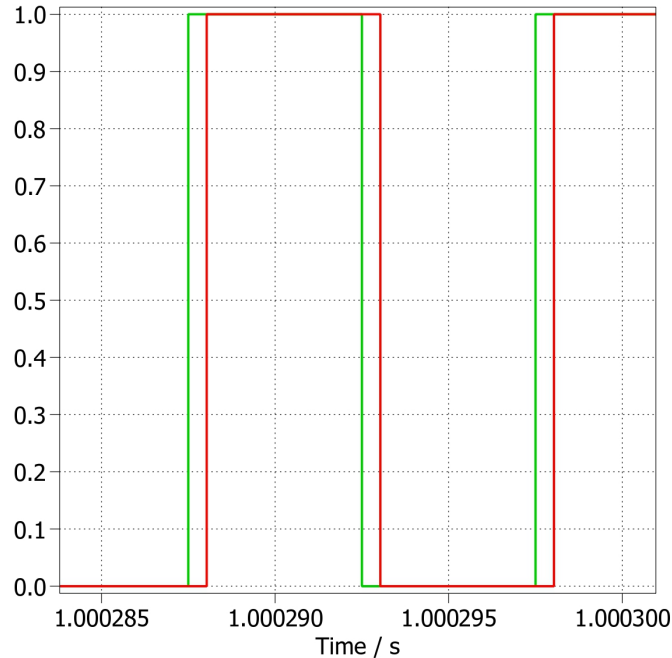


Figure 3.3: PWM Gate Signals for Forward Mode

current (Am4) during a segment of the steady-state operation of the converter. The primary voltage (red trace) is a bipolar square wave, switching between approximately +48 V and -48 V, indicative of the operation of the primary H-bridge, likely driven by a 50% duty cycle. The secondary voltage (green trace) is also a bipolar square wave, transitioning between approximately +400 V and -400 V, reflecting the voltage transformation by the isolation transformer and the switching of the secondary H-bridge. A phase shift is observable between the primary and secondary voltages, which is the control variable for power transfer in a DAB converter (primary H-bridge leads the secondary H-bridge). The inductor voltage (blue trace) is characterized by alternating positive and negative pulses, whose area determines the change in inductor current. Finally, the inductor current (black trace) is largely triangular, fluctuating around a positive DC offset, which is typical for power transfer from the lower voltage primary side to the higher voltage secondary side in this time frame. The relatively smooth and repetitive nature of these waveforms suggests stable operation during this period.

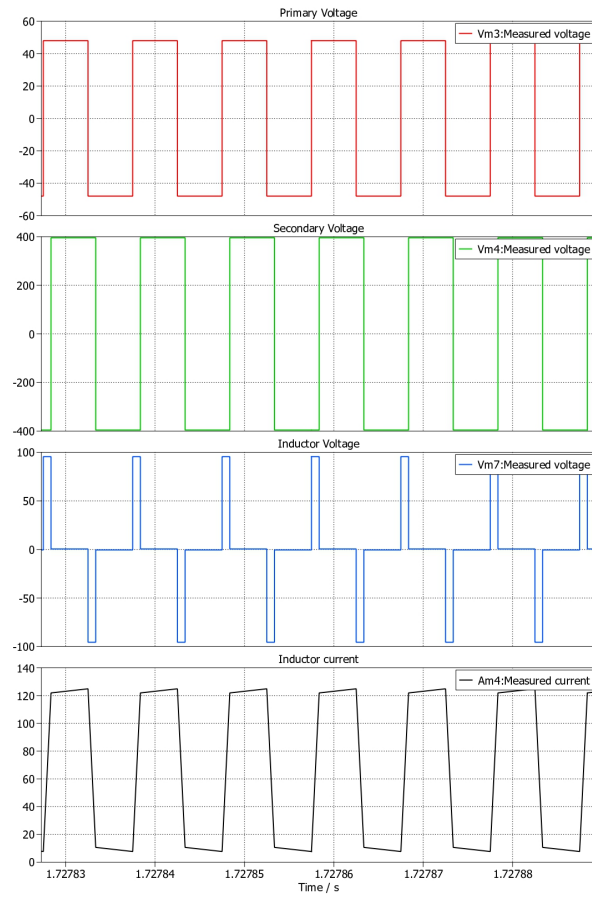


Figure 3.4: Waveforms of Primary Voltage, Secondary Voltage, Leakage Inductor Voltage, and Current

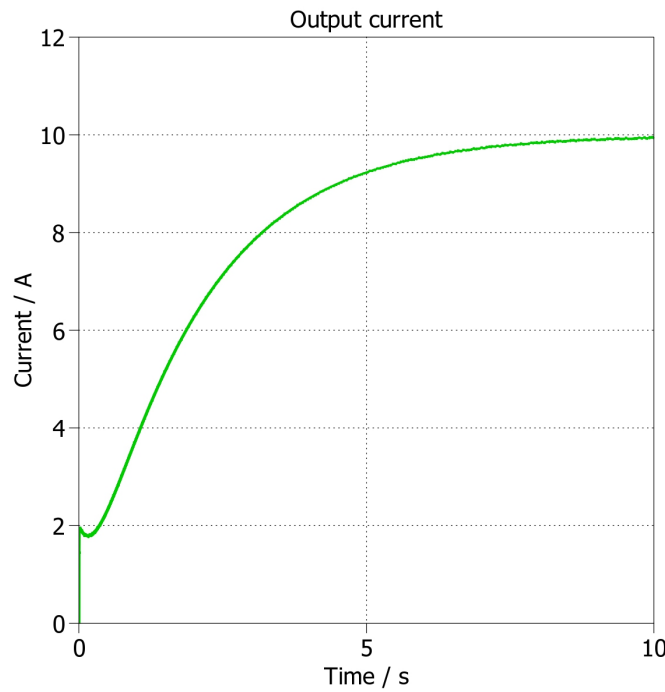


Figure 3.6: Output Current in forward Mode

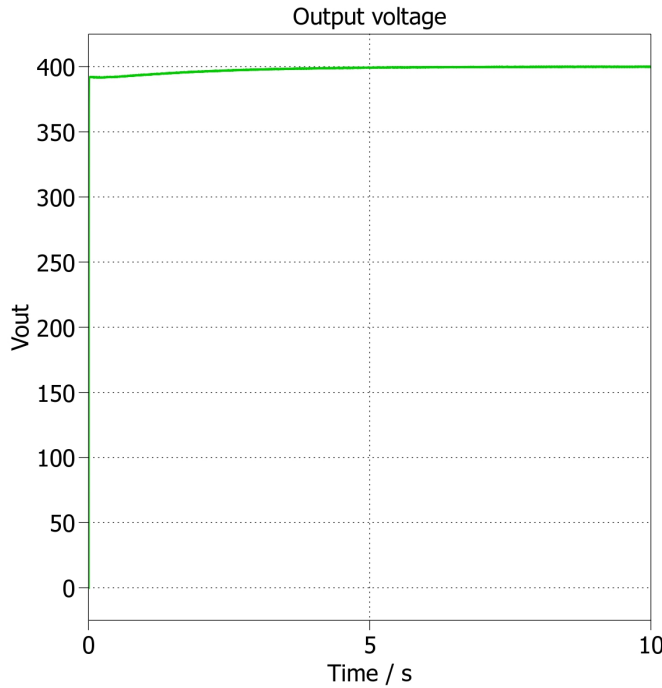


Figure 3.5: Output Voltage in forward Mode (48V to 400V)

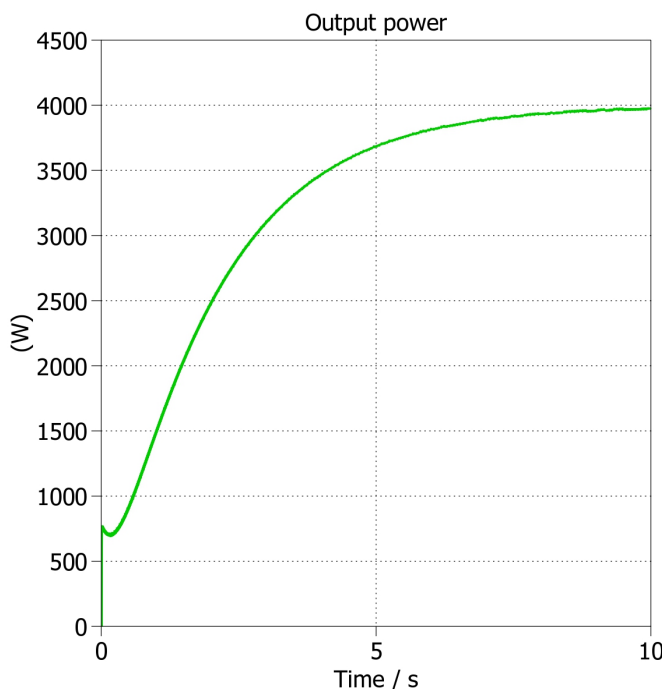


Figure 3.7: Power Waveform in forward Mode

3.8.2 Conclusion and Waveform Analysis for forward Mode(48 V to 400 V)

The simulation results for the forward mode (48V to 400V) demonstrate a successful low-to-high-voltage conversion. The output voltage waveform in Figure 3.5 shows a stable DC

voltage of approximately 400 V with minimal ripple, indicating effective voltage regulation. The output current waveform in Figure 3.6 reflects continuous conduction, with a smooth rise and fall corresponding to the switching intervals.

The measured output power is approximately 3965.9 W, which closely matches the intended 4 kW design target. The PWM signals in Figure 3.3 confirm that the primary side leads the secondary in phase, indicating forward power flow from low to high voltage. The timing and waveform symmetry validate that the phase-shift modulation is operating as intended, and the converter maintains efficiency and performance in this mode.

Stage 2: reverse Mode (High to Low Voltage)

Here, the converter transfers power from 400V (high voltage side) to 48V (low voltage side). The results show effective voltage regulation and stable operation.

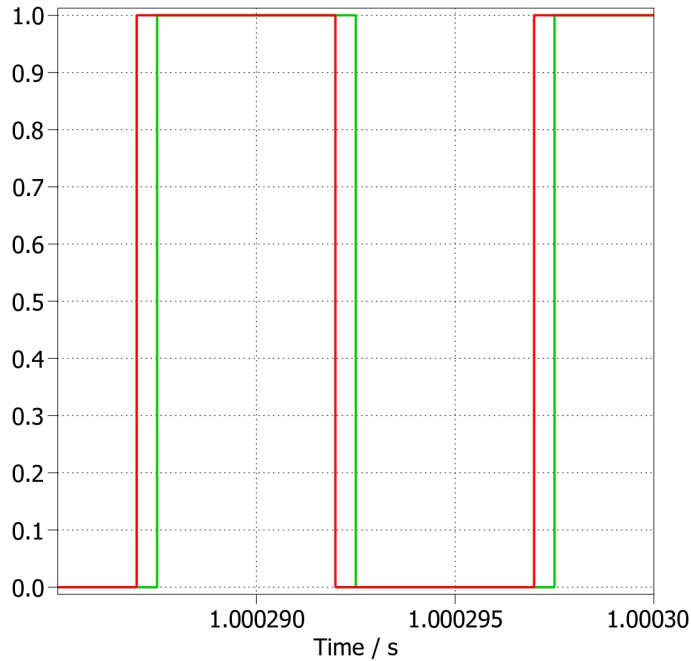


Figure 3.8: PWM Gate Signals for in reverse mode

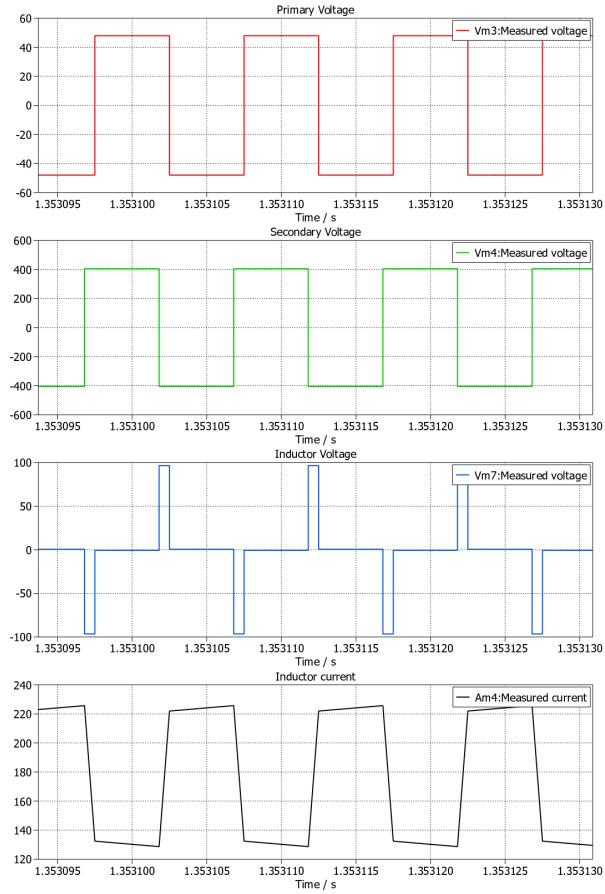


Figure 3.9: Waveforms of Primary Voltage, Secondary Voltage, Leakage Inductor Voltage, and Current

Figure 3.9 illustrates the converter waveforms during reverse mode operation. Both primary (Vm3, red trace) and secondary (Vm4, green trace) voltages display characteristic bipolar square waves at their respective voltage levels. In reverse mode, power flows from the higher voltage secondary side back to the lower voltage primary side, achieved by the secondary H-bridge voltage leading the primary H-bridge voltage. The inductor current (Am4, black trace) shows a triangular ripple, characteristic of the series inductor's role in facilitating bidirectional power flow between the two H-bridges. The consistent and periodic nature of these waveforms indicates stable operation in this reverse configuration.

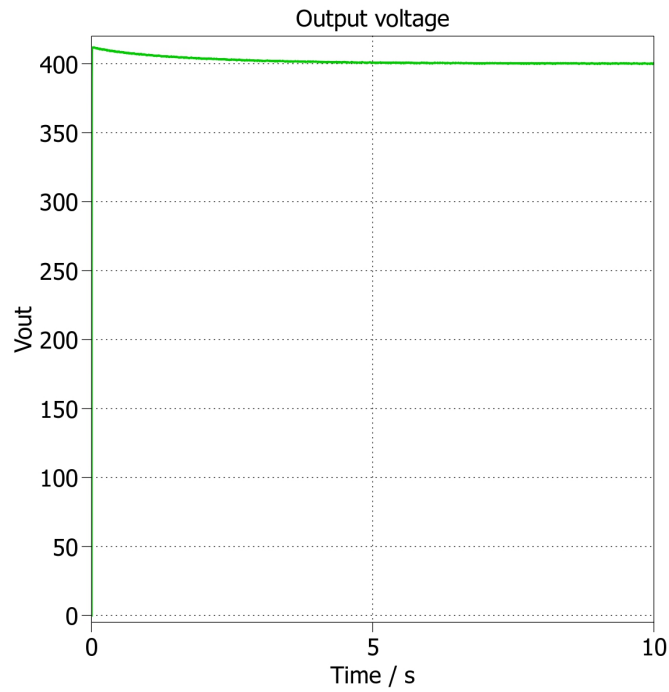


Figure 3.10: Output Voltage in reverse Mode (400V to 48V)

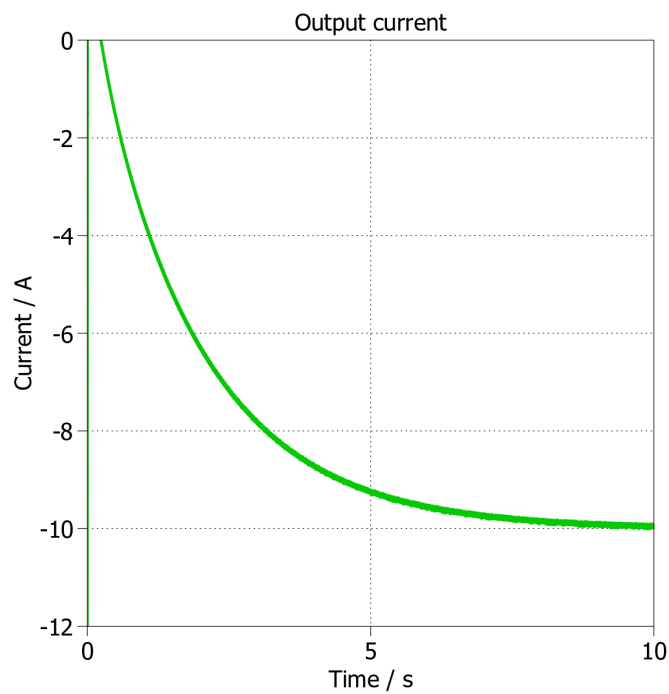


Figure 3.11: Output Current in reverse Mode

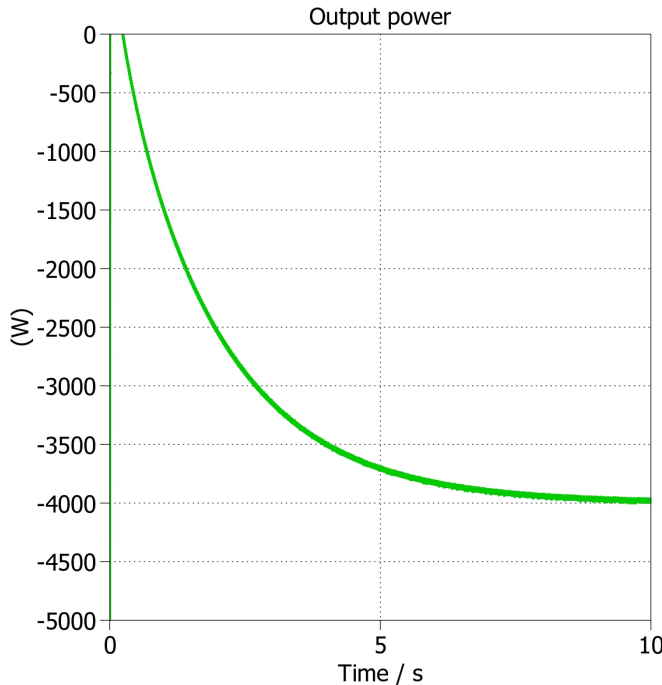


Figure 3.12: output power waveform in reverse mode

3.8.3 Conclusion and Waveform Analysis for reverse Mode (400 V to 48 V):

The simulation results for the reverse mode confirm effective high-to-low voltage conversion, with a power output of approximately -3965 W. The negative sign indicates power transfer from the high-voltage side (400 V) to the low-voltage side (48 V). In this mode, the secondary-side H-bridge leads the primary-side H-bridge in phase, establishing reverse power flow. The output current waveform exhibits continuous conduction with smooth transitions, consistent with expected reverse operation behavior.

The PWM gate signals (Figure 3.8) clearly illustrate the phase relationship between the bridges, demonstrating how the direction of power transfer is governed by the phase shift. Overall, the waveforms confirm that the converter operates reliably and efficiently under reverse mode conditions.

3.9 Discussion

The simulation results confirm the expected behavior of the DAB converter, including successful bidirectional power transfer. The output voltage remains stable during mode transitions. Transformer voltages and currents stay within safe operating limits, and the control system demonstrates a good dynamic response. The observed performance aligns with typical characteristics of high-frequency isolated converters.

Conclusion

This chapter presented the simulation results of the Dual Active Bridge (DAB) converter using PLECS. The converter was designed to operate bidirectionally between a low-voltage DC source (48V) and a high-voltage DC load (400V), with a targeted power transfer of 4kW at a switching frequency of 100kHz. The simulation validated the theoretical design by demonstrating correct operation in both forward and reverse modes. Key waveforms, including primary and secondary voltages, leakage inductor currents, and control signals, were analyzed to evaluate system performance. The results confirmed the effectiveness of phase shift control in managing power flow and highlighted the impact of transformer parameters and leakage inductance on the output. These simulations provided a solid foundation for the hardware implementation described in the following chapter.

CHAPTER 4

EXPERIMENTAL IMPLEMENTATION

Introduction

This chapter presents the implementation and experimental validation of the bidirectional Dual Active Bridge (DAB) converter. The setup includes all hardware components, measurement tools, and step-by-step testing methodology. Experiments include voltage validation, phase shift variation, and bidirectional operation.

4.1 Construction of the DAB Converter

The DAB converter was constructed using the following key components:

- **Transformer (5:10):** Used to step up voltage from 24V to 48V and provide galvanic isolation.
- **8 MOSFETs:** Four used in the primary full-bridge and four in the secondary full-bridge.
- **8 Gate Drivers:** Each MOSFET is driven by an isolated gate driver to ensure proper switching.
- **Input Capacitor:** Used to filter high-frequency ripple on the DC input voltage and supply instantaneous current during switching events.
- **Output Capacitor:** Used to smooth the output voltage on the secondary side.
- **Heat Sink Enclosure:** A metallic box was used to house the entire DAB converter. This enclosure acts as a large passive heat sink, absorbing and dissipating heat generated by all internal components, especially the MOSFETs, during operation.

The full-bridge circuits were connected on both sides of a high-frequency as shown in [4.1](#)

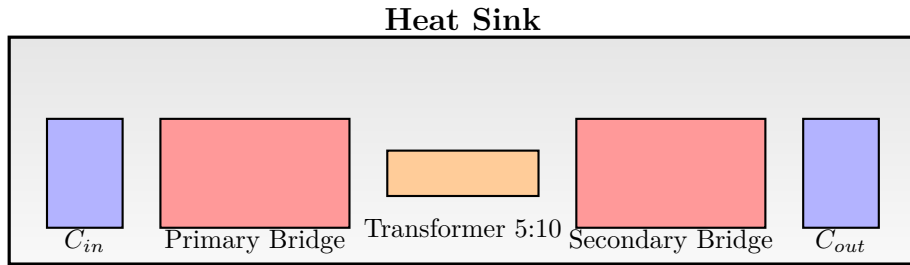


Figure 4.1: DAB converter diagram

The following image presents the real implementation of the DAB converter:

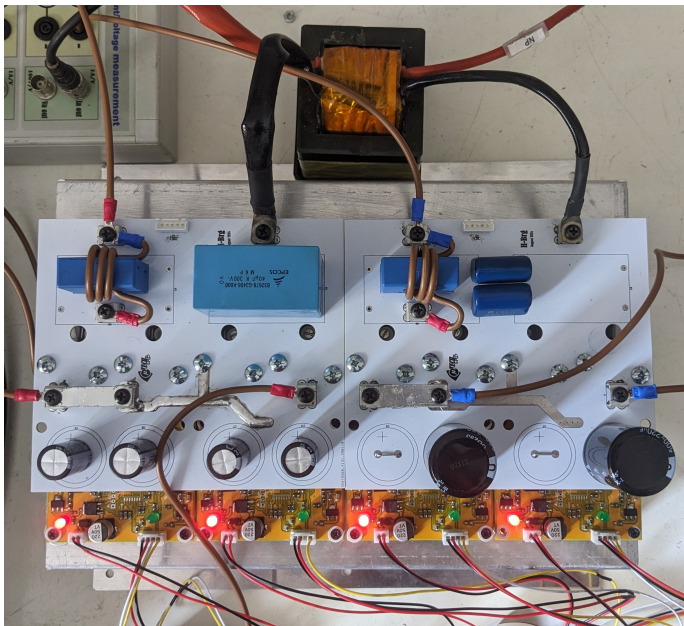


Figure 4.2: Hardware Implementation of the DAB Converter

4.2 Transformer Testing

4.2.1 Transformer Description

The transformer used in this project is a high-frequency ferrite-core transformer designed specifically for the Dual Active Bridge (DAB) converter. It plays a critical role in transferring power between the primary and secondary bridges while providing galvanic isolation and enabling bidirectional energy flow.

The core used is an **E70/33/32** ferrite core, chosen for its high magnetic permeability, compact size, and suitability for high-frequency operation. The E-core shape facilitates winding and mounting, while minimizing core losses at switching frequencies around 10kHz. A bobbin and insulating layers were used to separate windings and improve safety.



Figure 4.3: Transformer used in DAB converter.

4.2.2 Transformer Windings

The transformer is wound with a turns ratio of 5:10, meaning the primary winding consists of 5 turns and the secondary winding consists of 10 turns. This 1:2 turns ratio enables voltage step-up (from 24V to 48V) or step-down, depending on the direction of power flow. The number of turns was chosen based on the target voltage levels, desired flux density, and switching frequency, ensuring the transformer operates safely below its core saturation limit..

4.2.3 Leakage Inductance Measurement

The leakage inductance was measured using an **LCR meter** by shorting the secondary winding and measuring from the primary terminals. This test isolates the leakage component of the transformer inductance, which affects power transfer and ZVS behavior in the DAB topology. The measured leakage inductance was:

$$L_k = 3.9 \mu H$$

4.2.4 Addition of External Leakage Inductance

Although the measured leakage inductance of the transformer was $L_k = 3.9 \mu H$, this value was insufficient to regulate the high current flowing through the converter during full-power operation. In a DAB converter, the leakage inductance plays a critical role in shaping the inductor current and ensuring smooth power transfer between the bridges.

To mitigate the issue of excessive current and improve soft switching performance, an **external inductance of $177 \mu H$** was added in series with the primary side of the transformer. This additional inductance helped limit the peak current, reduce stress on the MOSFETs, and provide better control of the phase-shift modulation.

The total effective leakage inductance became:

$$L_{\text{total}} = L_k + L_{\text{external}} = 3.9 \mu H + 177 \mu H = 180.9 \mu H$$

This modification proved essential for stable and safe operation under high power levels.



Figure 4.4: External Leakage Inductance

4.2.5 Primary and Secondary Voltage Testing

The transformer was connected between the two full-bridge stages of the DAB converter and tested under switching operation. The following waveforms were captured using the oscilloscope:

- The **primary voltage** was observed as a square wave switching between +24V and -24V with a duty cycle based on phase shift.

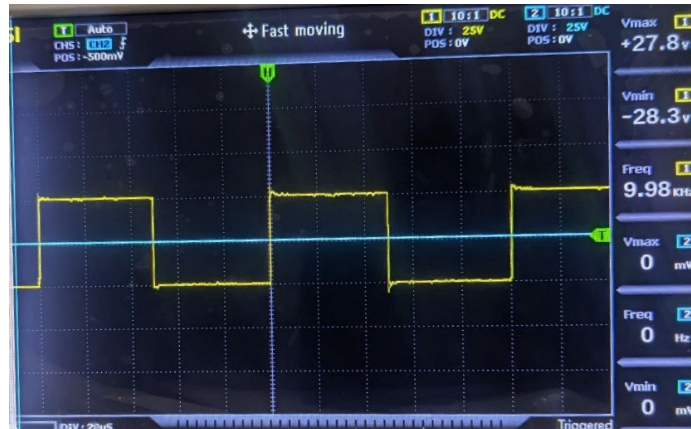


Figure 4.5: Primary side voltage waveform

- The **secondary voltage** followed the reflected waveform, stepping up the voltage and maintaining square wave shape due to high-frequency switching and low parasitics.



Figure 4.6: Secondary side voltage waveform

4.3 Materials and Equipment Used

- **Converter:** Bidirectional DAB
- **Batteries:** Two 12V NPP batteries connected in series to form 24V



Figure 4.7: Batteries

Served as the primary low-voltage input source (24V).

- **Output Load:** 100Ω



Figure 4.8: Output Load

A variable resistive load is connected to the secondary (high-voltage) side to evaluate converter performance, allowing for measurement of output voltage and current

- **Supercapacitor:** 10F on the secondary side



Figure 4.9: Supercapacitor 10F

Placed on the secondary side to test bidirectional energy transfer. It was charged during forward mode and discharged during reverse mode, allowing current direction to be observed.

- **Controller:** Texas Instruments C2000 MCU

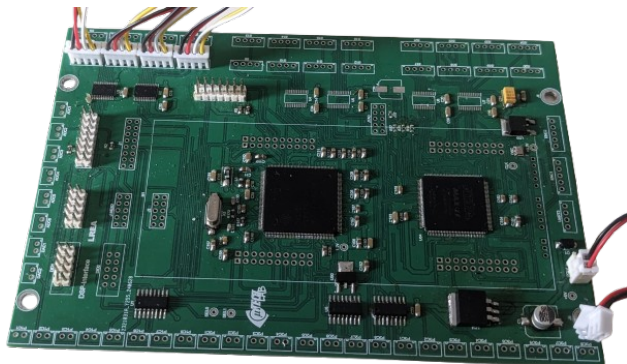


Figure 4.10: Texas Instruments C2000 MCU

It generated the phase-shifted PWM signals that controlled both full-bridge inverters of the DAB with a deadtime of 250 ns.

- **Oscilloscope:** Finirsi 1014D

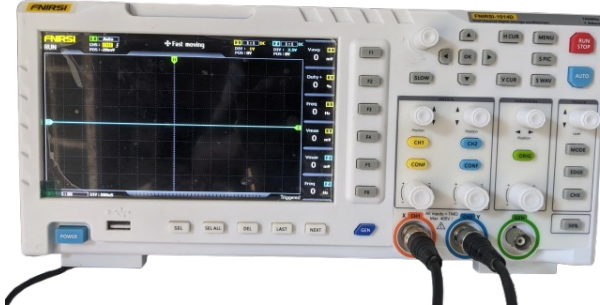


Figure 4.11: Finirsi 1014D Oscilloscope

Used to measure waveforms of voltages and currents in the DAB setup.

- **Measurement Modules:** Made by SARL Microtech (3-phase current/voltage)



Figure 4.12: Measurement Module

Installed on the input and output sides of the DAB converter to capture waveforms for current (input, output, inductor) and voltage measurements, all fed into the oscilloscope for analysis.

4.4 Experimental Setup

The experimental setup includes the power stage with the DAB topology, control board with C2000 controller, Measurement Modules, and oscilloscope connections. Proper heat sinks and isolation techniques were implemented to ensure safety and stability.

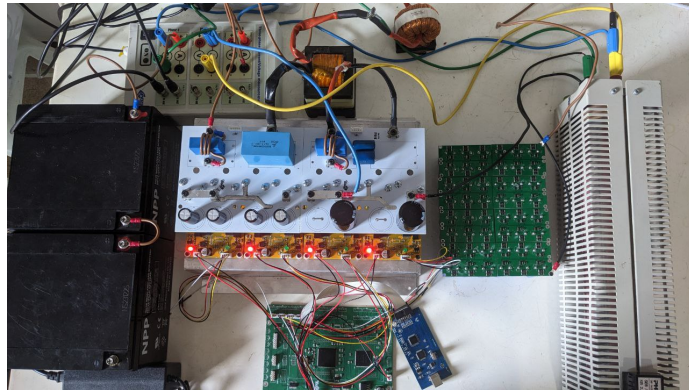


Figure 4.13: Photograph of the experimental setup

The above figure shows the complete experimental hardware, including the transformer, gate drivers, Measurement Modules, and oscilloscope probes. Proper wiring and insulation were applied to ensure stable operation and accurate measurements.

4.5 PWM Generation and Phase Shift Control

The PWM signals were generated using the ePWM modules of the TMS320F28379D. The controller enables precise control of phase shift to regulate power flow direction between the primary and secondary sides.



Figure 4.14: PWM signal for the primary side

This figure illustrates the generated PWM waveform for the primary bridge. A 50% duty cycle is used, and the frequency is set to 10 kHz, matching the DAB design specifications.



Figure 4.15: PWM signal for the secondary side

Secondary bridge PWM signal with fixed duty cycle and no internal phase shift. It receives a phase-shifted timing relative to the primary bridge to enable controlled power transfer across the transformer.

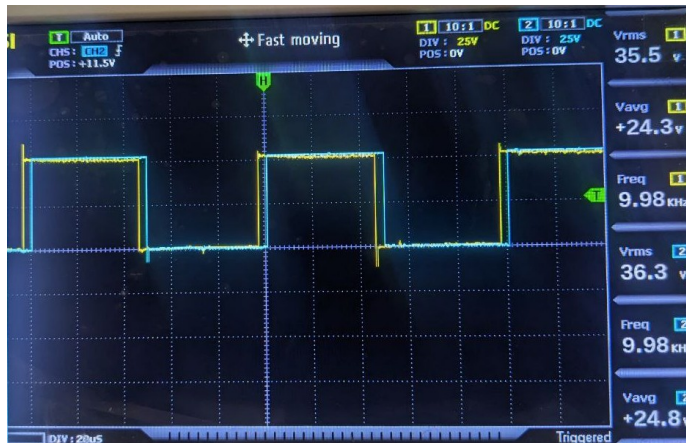


Figure 4.16: Phase shift between primary and secondary PWM signals

This waveform demonstrates the phase difference between the PWM signals of the two bridges. The magnitude and direction of this shift determine whether the power flows from primary to secondary or vice versa.

4.6 Phase Shift Variation Testing

This section analyzes the DAB response to different phase shifts: 0.1, 0.2, 0.3, and 0.4. For each phase shift, PWM, input/output currents, output voltage, and inductor current were measured.

4.6.1 Phase Shift = 0.1

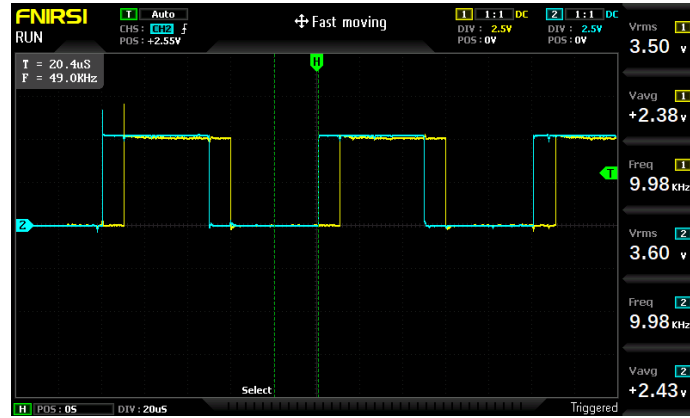


Figure 4.17: PWM Signal at Phase Shift 0.1



Figure 4.18: Input and Output Current at Phase Shift 0.1

Both input and output currents remain low, confirming low energy exchange.

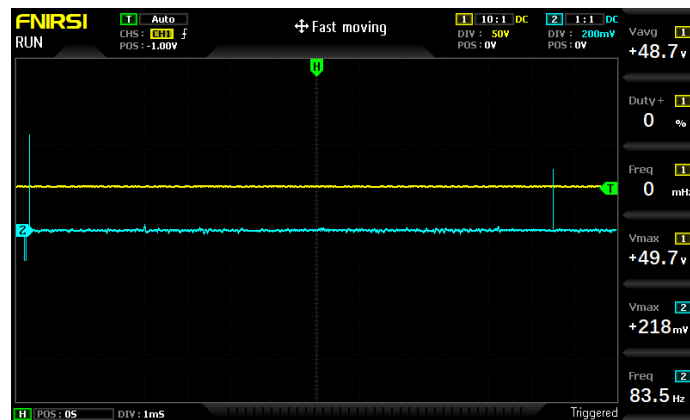


Figure 4.19: Output Voltage at Phase Shift 0.1

Output voltage stays below nominal due to the small transferred power.

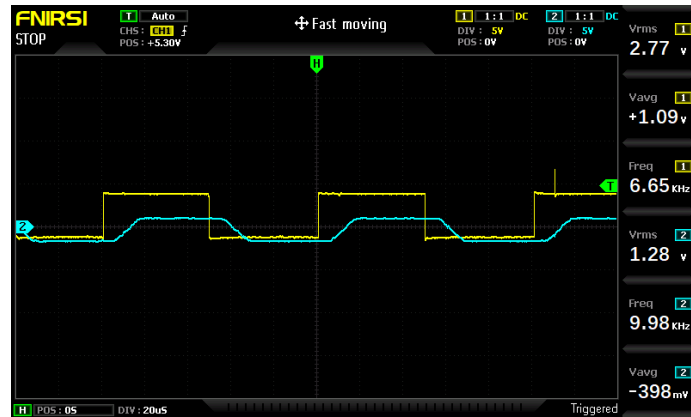


Figure 4.20: Inductor Current and PWM at Phase Shift 0.1

Low peak inductor current typical of limited transfer cycles at small phase shift.

4.6.2 Phase Shift = 0.2

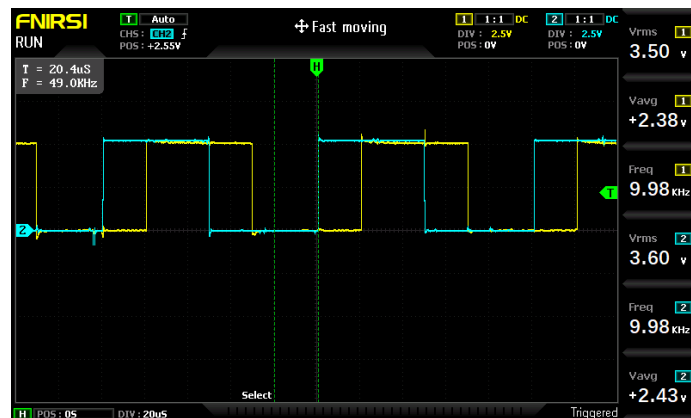


Figure 4.21: PWM Signal at Phase Shift 0.2



Figure 4.22: Input and Output Current at Phase Shift 0.2

Input and output currents increase significantly, indicating stronger power flow.

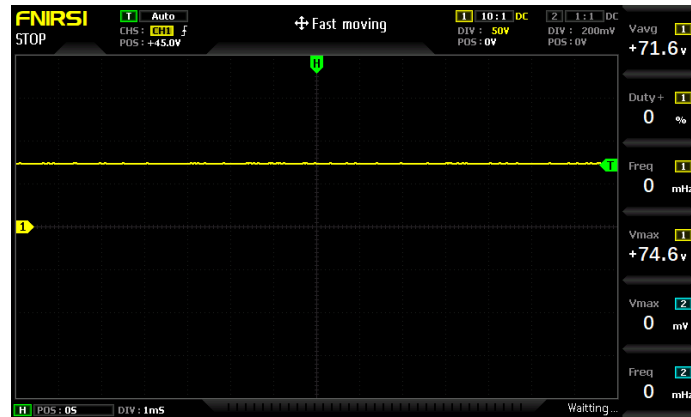


Figure 4.23: Output Voltage at Phase Shift 0.2

Output voltage rises proportionally to increased current and energy transfer.

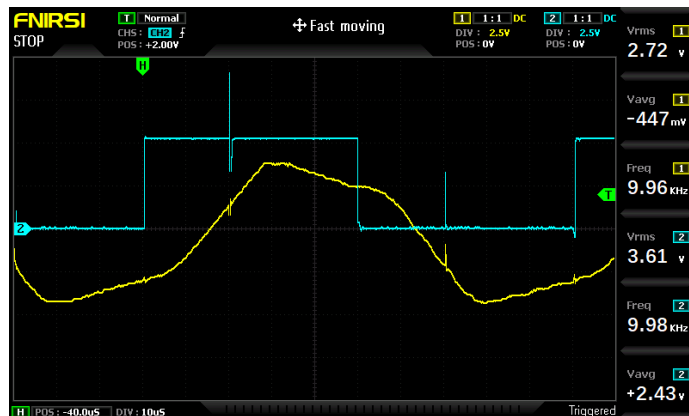


Figure 4.24: Inductor Current and PWM at Phase Shift 0.2

Inductor current increases and follows PWM overlap window.

4.6.3 Phase Shift = 0.3

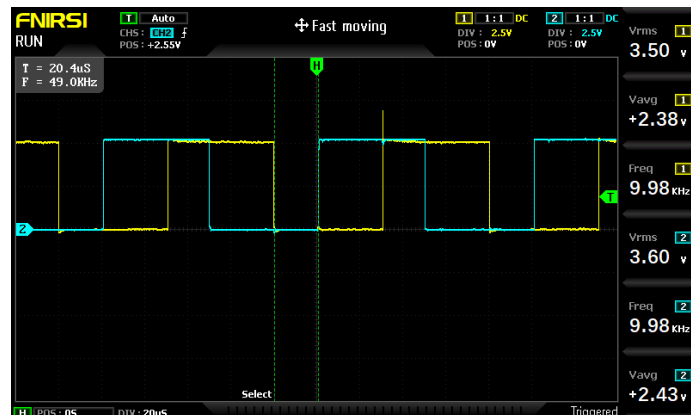


Figure 4.25: PWM Signal at Phase Shift 0.3



Figure 4.26: Input and Output Current at Phase Shift 0.3

The input and output current waveforms at a phase shift of 0.3 are comparable to those observed at 0.2, indicating a similar level of power transfer. The current profile is most likely symmetric to that of the 0.2 phase shift, reflecting the bidirectional nature of the DAB converter.

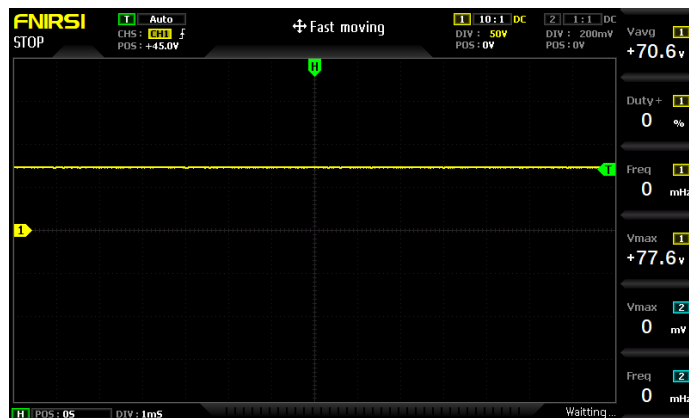


Figure 4.27: Output Voltage at Phase Shift 0.3

the output voltage stabilizes with reduced fluctuations, indicating steady-state operation

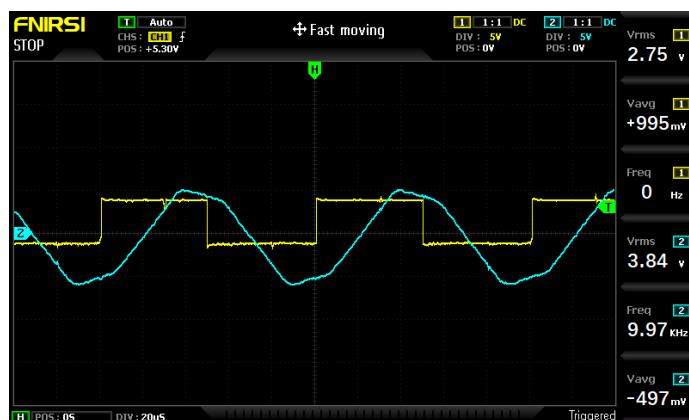


Figure 4.28: Inductor Current and PWM at Phase Shift 0.3

Peak inductor current increases, indicating stronger energy delivery.

4.6.4 Phase Shift = 0.4

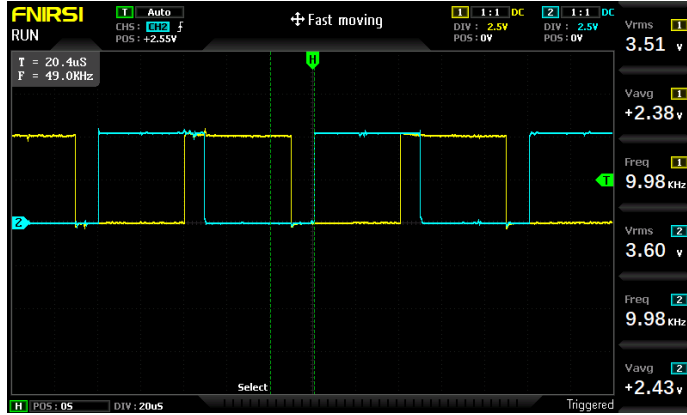


Figure 4.29: PWM Signal at Phase Shift 0.4



Figure 4.30: Input and Output Current at Phase Shift 0.4

At a phase shift of 0.4, the output current expectedly decreases and resembles the current profile observed at 0.1 phase shift. This behavior reflects the symmetric nature of power transfer in the DAB

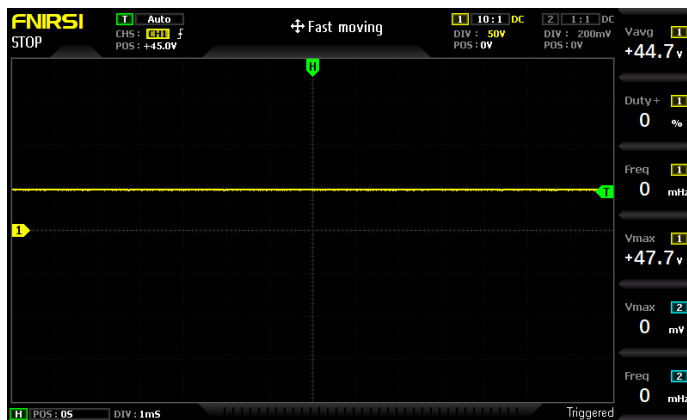


Figure 4.31: Output Voltage at Phase Shift 0.4

Output voltage decreases, confirming lower effective power transfer at large phase shift.

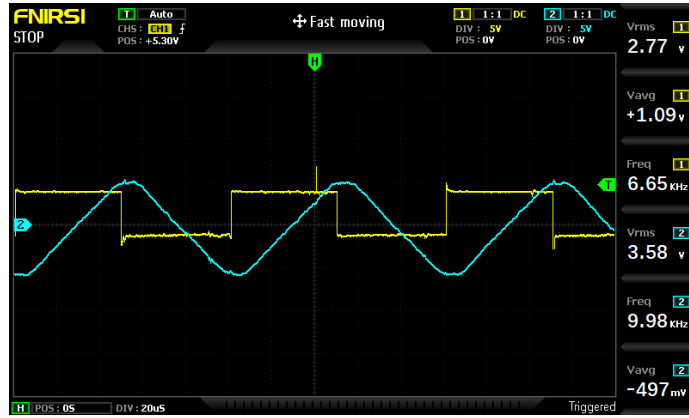


Figure 4.32: Inductor Current and PWM at Phase Shift 0.4

The inductor current is higher due to increased circulating (reactive) power, but less real power is delivered to the load.

Table 4.1: Measured DAB Parameters at Different Phase Shifts

Phase Shift	I_{in} (A)	I_{out} (A)	V_{out} (V)	Peak I_L (A)	P out (W)
0.1	3	0.511	49.7	1.28	24.7
0.2	2.62	0.710	74.6	3.61	55.652
0.3	3.05	0.772	77.6	3.84	60.22
0.4	1.69	0.465	47.7	3.58	22

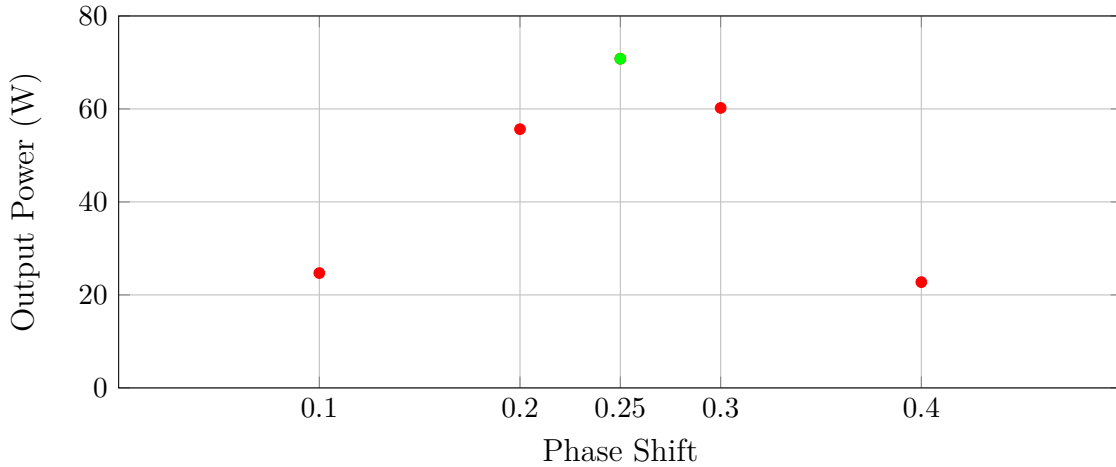


Figure 4.33: Output Power as a Function of Phase Shift in the DAB Converter

4.6.5 Discussion: Phase Shift Variation Results

The experimental analysis of phase shift variation highlights the fundamental operating principle of the Dual Active Bridge (DAB) converter, where power transfer is governed by the phase difference between the primary and secondary bridge PWM signals. As shown

in Table 4.1, increasing the phase shift from 0.1 to 0.3 resulted in greater output voltage, current, and total output power, consistent with the theoretical characteristics of Single Phase Shift (SPS) control.

At a low phase shift of 0.1, the PWM overlap between primary and secondary bridges is minimal, producing only a narrow power transfer window. Consequently, the converter delivered just 24.7 W, with an output voltage of 49.7 V and a peak inductor current of 1.28 A. This behavior reflects low effective energy exchange and limited magnetizing energy across the transformer.

Increasing the phase shift to 0.2 significantly expanded the effective conduction window. The resulting rise in both output voltage (74.6 V) and current (0.71 A) doubled the output power to 55.65 W. At phase shift 0.3, performance peaked with 60.22 W output power, 77.6 V output voltage, and 0.772 A current. The inductor current also peaked at 3.84 A. This confirms that, in this SPS-controlled system, the maximum real power transfer occurs near a normalized phase shift of 0.25–0.3, as predicted by the ideal relation:

$$P \propto \phi(1 - \phi) \quad (4.1)$$

where ϕ is the normalized phase shift.

At a phase shift of 0.4, the output power dropped to 22.75 W, and the voltage fell to 47.7 V. Although this might appear as a performance anomaly, it actually follows the theoretical curve: after $\phi = 0.25$, the product $\phi(1 - \phi)$ decreases, leading to lower transferred power. While the inductor current remained high (3.58 A), this includes a larger reactive component that does not contribute to real power transfer. Additionally, operating far from the optimal point may lead to increased switching and conduction losses, reduced ZVS margins, and elevated transformer magnetization currents, all of which contribute to reduced efficiency.

Furthermore, non-ideal factors—such as device mismatches, core losses, and measurement limitations—can distort the current and voltage waveforms, especially in open-loop configurations like this one. The measurement board used for voltage and current sensing was aged and partially damaged, which affected the accuracy of some results, particularly at higher phase shifts.

In conclusion, the measured results confirm the sinusoidal-like power transfer profile predicted by theory. The DAB converter achieves maximum real power transfer near a phase shift of 0.25, with efficiency degrading beyond this point due to both theoretical and practical factors. The system effectively demonstrates the viability of SPS control for bidirectional energy applications.

4.7 Bidirectional Operation Testing

To verify the bidirectional operation of the implemented Dual Active Bridge (DAB) converter, an open-loop test was conducted. The system was configured to operate between 24 V (primary side) and 48 V (secondary side). On the secondary side, a large 10 F capacitor was connected in parallel with a $100\ \Omega$ resistive load to simulate realistic charging and discharging conditions.

The test was performed by sweeping the phase shift from $+0.1$ to -0.1 , enabling power flow in both directions depending on the phase polarity.

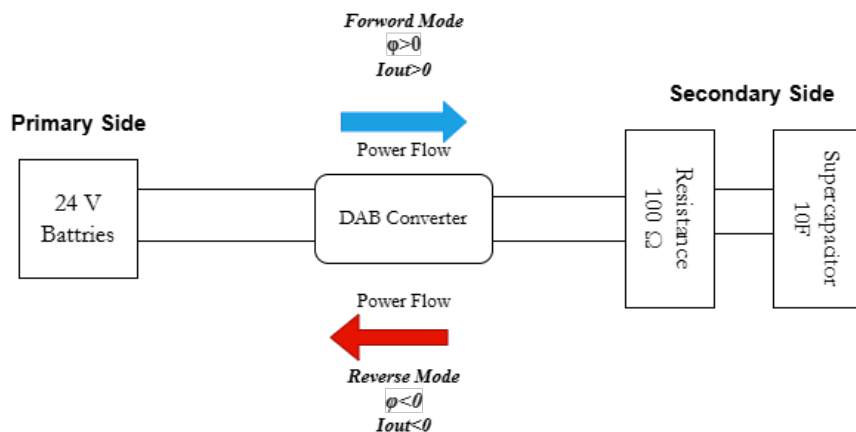


Figure 4.34: Experimental Setup for Bidirectional Power Transfer in DAB Converter

4.7.1 Forward Mode (Charging the Capacitor and Supplying the Load)

In Forward mode, a positive phase shift ($+0.1$) was applied, transferring power from the 24 V primary side to the 48 V secondary side. The 10 F capacitor on the secondary began charging, and the $100\ \Omega$ load drew current simultaneously.

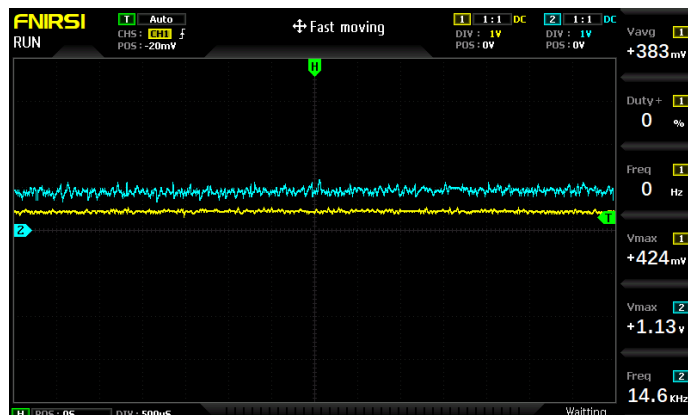


Figure 4.35: Output current in forward mode

The oscilloscope trace shows positive current flow on the primary side, indicating successful power transfer toward the secondary. Even without direct capacitor voltage monitoring, the load presence and current direction confirm capacitor charging and load supply.

4.7.2 Reverse Mode (Discharging the Supercapacitor and Transferring Power Back to the Input Side)

In reverse mode, a negative phase shift (**-0.1**) was applied. This reversed power flow from the 48V secondary to the 24V primary side. The 10F capacitor discharged through the 100Ω resistor, supplying the load and sending energy back to the source.



Figure 4.36: output current in reverse mode.

The oscilloscope shows negative current flow, clearly verifying the DAB's ability to support reverse power transfer and capacitor discharge.

4.7.3 Discussion

The current direction captured by the oscilloscope positive during forward and negative during reverse confirms the bidirectional operation of the Dual Active Bridge converter. Although voltage plots were unavailable, the current waveforms, controlled by phase shift changes, demonstrate clear energy flow in both directions. The load and capacitor behavior during these modes shows the DAB is effective for DC energy storage applications, power balancing, and reversible systems such as electric vehicle chargers and renewable integration.

4.7.4 Efficiency Calculation

The efficiency of the DAB converter can be calculated using the ratio of output power to input power:

$$\eta = \frac{P_{\text{out}}}{P_{\text{in}}} \times 100\% \quad (4.2)$$

Given:

$$V_{\text{in}} = 24 \text{ V}, \quad I_{\text{in}} = 2.62 \text{ A}, \quad V_{\text{out}} = 74.6 \text{ V}, \quad I_{\text{out}} = 0.710 \text{ A}$$

$$P_{\text{in}} = V_{\text{in}} \times I_{\text{in}} = 24 \times 2.62 = 62.88 \text{ W}$$

$$P_{\text{out}} = 74.6 \times 0.710 = 52.966 \text{ W}$$

$$\eta = \frac{52.966}{62.88} \times 100 = 84.2\%$$

Result: The efficiency is approximately **84.2%**.

Conclusion

This chapter presented the practical implementation and experimental validation of the Dual Active Bridge (DAB) converter designed to operate between 24V and 48V. Detailed testing was carried out to evaluate the converter's performance under various operating conditions.

Phase shift variation tests demonstrated the expected power modulation behavior of the DAB, with output power peaking near a 0.25 phase shift and decreasing for lower and higher values. The measurements of input/output currents, voltages, and inductor current aligned with theoretical expectations, confirming proper energy transfer characteristics. However, it should be noted that the current and voltage sensors used were outdated and partially damaged, which likely affected the accuracy of the measured current and output voltage values.

Additionally, the bidirectional nature of the DAB was successfully validated using a 10 F supercapacitor and 100Ω load on the secondary side. Oscilloscope traces of current direction clearly confirmed energy flow in both forward and reverse modes.

Despite the measurement limitations, the experimental work successfully demonstrated the fundamental operation of the DAB converter. The results confirm the converter's potential for applications requiring bidirectional DC energy flow, such as battery systems, electric vehicles, or renewable energy interfaces.

CHAPTER 5

GENERAL CONCLUSION

In conclusion, this thesis demonstrated the successful design, simulation, and experimental validation of a bidirectional Dual Active Bridge (DAB) DC-DC converter. The converter operated effectively between 48 V and 400 V in simulation and was experimentally tested over a 24 V to 48 V range. The use of Single Phase Shift (SPS) control and a PI-based controller enabled efficient and stable power transfer in both directions. From a practical perspective, the DAB topology offers key advantages in terms of compact size, reduced component stress, and suitability for high-frequency operation, which collectively contribute to lower overall system size and cost. Additionally, by minimizing switching losses and optimizing control timing including deadtime the converter achieved improved efficiency, making it a strong candidate for applications such as renewable energy systems, battery storage, and electric vehicle power interfaces. This work provides a solid foundation for future enhancements, including higher power scaling, more advanced control methods, and integration into real-world energy systems.

Future Work

Although the proposed system has achieved its primary objectives, several areas remain open for future improvement and exploration:

- **Advanced Control Strategies:** Implement and compare more sophisticated control algorithms such as Dual Phase Shift (DPS), Model Predictive Control (MPC), or Artificial Intelligence-based controllers for improved efficiency and dynamic response.
- **Digital Implementation Optimization:** Investigate the use of faster or more resource-efficient digital platforms such as FPGAs for real-time control with high switching frequencies.
- **Thermal Management and Efficiency Analysis:** Perform detailed thermal modeling and efficiency profiling under varying load conditions to optimize the design for industrial applications.
- **Multi-port Extension:** Extend the system to a multi-port configuration for integration with hybrid energy sources such as solar panels, batteries, and supercapacitors.
- **Fault Detection and Protection:** Integrate protection features and real-time fault detection mechanisms to enhance the reliability of the converter in practical applications.

In conclusion, the work presented in this thesis provides a solid foundation for future developments in high-performance bidirectional DC-DC power conversion systems.

BIBLIOGRAPHY

- [1] P. Sharma, D. Palwalia, and A. Sharma, “A review: Bi-directional dc-dc converter topologies,” *International Journal of Technical Research Science*, vol. 9, pp. 27–35, 06 2024.
- [2] S. A. Gorji, H. G. Sahebi, M. Ektesabi, and A. B. Rad, “Topologies and control schemes of bidirectional dc–dc power converters: An overview,” *IEEE Access*, vol. 7, pp. 117997–118019, 2019.
- [3] D. Li and S. Luo, “Sepic and zeta converters with reduced input current ripple for fuel cell power system,” *IEEE Transactions on Industry Applications*, vol. 39, no. 4, pp. 1135–1140, 2003.
- [4] T. Wu, Y. Chen, and Y. Huang, “Non-isolated bidirectional cuk converter for battery energy storage systems,” *IEEE Transactions on Industrial Electronics*, vol. 57, no. 10, pp. 3465–3474, 2007.
- [5] K. C. Tseng and C. C. Huang, “High-efficiency bidirectional converter for energy storage systems,” *IEEE Transactions on Industrial Electronics*, vol. 46, no. 4, pp. 758–765, 1999.
- [6] M. Zhu and F. Gao, “Review on bidirectional dc–dc converters for renewable energy systems,” *IEEE Transactions on Power Electronics*, vol. 28, no. 4, pp. 556–566, 2013.
- [7] Y. Liu, F. Peng, and X. Li, “Digital control of bidirectional dc-dc converters for energy storage systems: A review,” *IEEE Access*, vol. 7, pp. 50520–50534, 2019.
- [8] S. Lee, P. Barbosa, and P. T. Krein, “Bidirectional flyback converter design for fuel cell systems,” *IEEE Transactions on Power Electronics*, vol. 21, no. 4, pp. 1145–1155, 2006.
- [9] S. Baek, C. Yoo, and J. Lee, “Bidirectional forward dc-dc converter for fuel cell application,” *IEEE Transactions on Power Electronics*, vol. 20, no. 6, pp. 1271–1279, 2005.

BIBLIOGRAPHY

- [10] D. M. D. R. W. De Doncker and M. H. Kheraluwala, “A three-phase soft-switched high-power-density dc-dc converter for high power applications,” *IEEE Transactions on Industry Applications*, vol. 27, no. 1, pp. 63–73, 1991.
- [11] W. Shen, C. Zhao, and J. Wang, “Review of high-frequency bidirectional isolated dc-dc converters for bidirectional battery chargers,” *IEEE Transactions on Industrial Electronics*, vol. 64, no. 4, pp. 2518–2528, 2018.
- [12] A. K. Jain and R. Ayyanar, “Pwm control of dual active bridge: Comprehensive analysis and experimental verification,” *IEEE Transactions on Power Electronics*, vol. 26, no. 4, pp. 1215–1227, 2011.
- [13] F. Krismer and J. W. Kolar, “Efficiency-optimized high-current dual active bridge converter for automotive applications,” *IEEE Transactions on Industrial Electronics*, vol. 59, no. 7, pp. 2745–2760, 2012.
- [14] H. Tao, J. L. Duarte, and M. A. M. Hendrix, “Multi-phase bidirectional dc-dc converter with full zvs range and enhanced power density,” *IEEE Transactions on Power Electronics*, vol. 23, no. 2, pp. 782–792, 2008.
- [15] Z. Chen, D. Xu, and J. Zhang, “A model predictive control strategy for dual-active-bridge dc-dc converters to improve the transient response,” *IEEE Transactions on Power Electronics*, vol. 33, no. 4, pp. 3637–3651, 2018.
- [16] M. F. Sulaiman, N. A. Rahim, and H. W. Ping, “Advanced control strategy of bidirectional dc-dc converter for renewable energy application,” *IET Power Electronics*, vol. 9, no. 7, pp. 1401–1411, 2016.
- [17] S. Kouro, M. Malinowski, K. Gopakumar, J. Pou, L. G. Franquelo, B. Wu, J. Rodriguez, M. A. Pérez, and J. I. Leon, “Model predictive control—a review of its applications in power electronics,” *IEEE Transactions on Industrial Electronics*, vol. 56, no. 6, pp. 1826–1838, 2009.
- [18] R. Biswash, “Design and implementation of high-frequency dc-dc converters for ev applications,” M.S. thesis, University of Arkansas, Fayetteville, May 2024, available at: <https://scholarworks.uark.edu/etd/5328/>.
- [19] V. M. Iyer, G. Narayanan, and V. Ramanarayanan, “Small-signal stability assessment and active stabilization of a bidirectional battery charger,” *IEEE Transactions on Industry Applications*, vol. 55, no. 1, pp. 563–574, 2019.

APPENDICES

Appendix A: PLECS Simulation

This appendix provides detailed information regarding the PLECS simulation model of the bidirectional Dual Active Bridge (DAB) DC-DC converter

<https://github.com/simony23-art/DAB-simulation.git>

Appendix B: TI C2000 Documentation

Technical reference manual and datasheet of the Texas Instruments C2000 microcontroller used in the control implementation.

<https://www.ti.com/product/TMS320F28379D>

Appendix C: Gate Driver Information

Specifications of the gate driver used to control the SiC MOSFETs. Further details can be accessed at:

<https://www.ti.com/product/IS05852S>

Appendix D: Transformer Core Data

Magnetic and dimensional characteristics of the EE70-70 core transformer used in the prototype.

https://www.tdk-electronics.tdk.com/inf/80/db/fer/e_70_33_32.pdf

Appendix F: Voltage Sensor (Measurement) Modules

The converter uses two voltage divider-based sensing circuits for measuring high-voltage signals. For detailed component specifications and application examples, refer to:

<https://www.ti.com/product/TLV700>

Appendix G: Current Sensor LA55-P

The current measurement in the system is performed using the LA55-P Hall effect sensor. More information can be found on the manufacturer's website:

<https://datasheet.ciiva.com/26928/la55-p-26928790.pdf>

Appendix H: PLECS Simulation

This appendix provides documentation of PLECS simulator used to build our simulation.

<https://www.plexim.com/download/documentation>

Appendix I: Implementation results

This appendix provides videos and pictures of the experiment provided in chapter 5

<https://github.com/simony23-art/DAB.git>